Interaction of Amphiphilic Gold Nanoparticles with Lipid Membranes and Their Application to Cancer Radiotherapy

By

Yu-Sang Yang

B.S. Materials Science and Engineering
National Tsing Hua University, 2010

SUBMITTED TO THE DEPARTMENT OF
MATERIALS SCIENCE AND ENGINEERING IN
PARTIAL FULFULLMENTS FOR THE DEGREE OF

MASTER OF SCIENCE IN MATERIALS SCIENCE AND ENGINEERING
AT THE
MASSACHUSETTS INSTITUTE OF TECHNOLOGY

June 2013

Signature of Author _____
Department of Materials Science and Engineering
May 6th, 2013

Certified by _____
Darrell J. Irvine
Professor of Materials Science and Engineering and Biological Engineering
Thesis Supervisor

Accepted by _____
Gerbrand Ceder
Chair, Departmental Committee on Graduate Student

Interaction of Amphiphilic Gold Nanoparticles with Lipid Membranes and Their Application to Cancer Radiotherapy

By

Yu-Sang Yang

Submitted to the Department of Materials Science and Engineering
on May 6th, 2013 in Partial Fulfillment of the
Requirements for the Degree of Master of Science in
Materials Science and Engineering

ABSTRACT

Striped gold nanoparticles (NPs), inorganic particles protected by an amphiphilic mixed organic ligand shell, are the most recent and potent evolution of gold nanoparticle intracellular delivery vectors. Here we propose the combination of striped gold nanoparticles with lipid vesicles of diameter < 200 nm in order to concentrate their delivery and couple their delivery to the delivery of pharmaceuticals. Mechanisms of penetration of striped gold nanoparticles into live cell membranes via non-endocytic pathways was poorly understood, therefore this work focuses on the interaction of striped NPs with synthetic lipid membranes as models for cellular membranes, and interactions with bacterial membranes have been investigated to provide a more stringent test of their interaction capacity. Cellular uptake of striped gold nanoparticles has been observed to be homogeneous when delivered via interbilayer crosslinked multilamellar lipid vesicles, which resulted in enhancement of striped gold nanoparticle induced radiosensitization causing membrane rupture and genomic damage.

Thesis Supervisor: Darrell J. Irvine
Title: Professor of Materials Science and Engineering and Biological Engineering

ACKNOWLEDGEMENTS

First and foremost, I would like to acknowledge my advisor Professor Darrell Irvine for the mentorship, guidance, trust, and freedom he has given me. Without him, this work would not have been possible. His creativeness, intelligence, patience and enthusiasm have inspired me professionally and personally, leading me to becoming a "hardcore" scientist. Data analysis and brainstorming with Darrell and the research group have been among the most enjoyable moments at work.

Needless to say, many people's efforts have made this work possible. I would like to thank Randy Carney and Professor Stellacci for the constant supply of striped gold nanoparticles and sage advice. I will never forget the impromptu and inspiring discussion about nanoparticle-membrane interactions with Professor Stellacci when he visited MIT. I am very grateful to have had the opportunity to collaborate with Sebastian and Professor Lu on the bacterial membrane project. Also, I would like to thank Nicki for her help on ultramicrotomy. Special thanks to Reid and Professor Alexander-Katz for the exciting collaboration on studying the mechanism of lipid membrane interaction with striped nanoparticles through comparison of modeling and experimental result. Thanks, Dave—the thesis would not have been as rigorously objective as it is without editing with you.

I owe special thanks to the Irvine lab members, who have made 76-211 a wonderful place to work at. Thanks to Haipeng, Prabhani, James, Adrienne, and Erin who helped me get started in the lab. Thanks to Suhda, Kavya, Talar, Pete, Greg, Ana, Melissa, Chyan-Ying, Yiran, Sharon, Mila, Brad, Bonnie, Maria, Heikyung and Wuhbet for their help and discussion.

I will never forget my quals prep friends Binghong and Zhouhong for their kind unofficial TA hours during stressful times. Life as a graduate student in MIT has been very challenging yet enjoyable. Thanks to my best friends, Sheng-Po Hsia, Ritchie Chen, Corentin Monmeyran, Brent Keller, Geran Zhang and all the DMSE 16' thread friends for the fun times and distractions.

I would like to thank my undergraduate advisors Professor Dar-Bin Hsieh and Professor Chia-Chun Chen for their dedicated support, mentorship, and nourishment of my deep interest in science that brought me to where I am now.

Last but not certainly not least, thank you my family for the love and support throughout my entire life. The short sentence can never express my gratitude and love to you.

TABLE OF CONTENTS

List of Figures

1 Introduction

1.1 Gold Nanoparticle Applications in Biomedical Research

Since their discovery, the potential of gold nanoparticles for clinical treatments has been the subject of extensive investigation. Gold nanoparticles coated with biocompatible ligands have tunable sizes, shapes, and optical properties [14]. Recent advances in the synthesis, surface functionalization, and biocompatibility of gold nanoparticles have motivated studies of their application as drug carriers, imaging contrast agents, immunostaining, photoresponsive therapeutics, and radiosensitizers [18].

Bioconjugation of oligonucleotides, pharmaceuticals, or proteins on gold nanoparticle surfaces can make these nanomaterials an efficacious vector for pharmaceutical delivery. Surface ligands, charge, and size of gold nanoparticles play important roles in the toxicity and delivery efficiency [23]. Biomedical scientists continue to investigate functionalization of cell-penetrating peptides on gold nanoparticle surfaces for trans-membrane delivery of macromolecules [36].

Antibody-modified Au particles immunostain cellular antigen, guided by molecular recognition. Compared to fluorescence labeling, gold nanoparticles do not suffer from photobleaching which is a major limitation for fluorescence based imaging, and in the case of TEM imaging better resolution with high contrast can be obtained. Gold nanoparticles can be used to improve contrast when imaging via X-ray computer tomography. The high-Z material allows for short exposure times while achieving a high signal-to-noise ratio and reducing radiation damage to surrounding tissues [21].

Gold nanoparticles can also intrinsically act as therapeutics without conjugation to drugs. Gold particles are thermally excited by specific wavelength bands of light. Selective loading of gold nanoparticles onto target tissues allows for their hyperthermic destruction without damaging surrounding tissues [24].

In radiotherapy, the high X-ray absorption cross section of gold exploited, lending itself to clinical application as a highly localized radiation target. *In vivo* treatment of mice with gold nanoparticles and subsequent X-ray irradiation resulting in an 86% long-term survival rate. The control group that underwent irradiation in the absence of gold nanoparticle treatments had a 20% long-term survival rate [20].

Gold nanoparticles facilitate a broad range of clinical applications utilizing their atomic and unique chemical properties. Targeting schema, X-ray sensitization, and pharmaceutical delivery via gold nanoparticle have been the focus of extensive biomedical investigation. Realization of viable clinical applications must overcome limited *in vivo* targeting delivery efficiency. Manifold means by which to improve targeting delivery efficiency are under investigation and are the subject of this work.

1.2 Features of "Striped" Gold Nanoparticles

Gold nanoparticles used in biomedical applications are typically solubilized in aqueous solution via capping with an organic ligand layer (Figure 1-1). A variety of organic ligand shells have been used in prior studies, including tiopronin, glutathione, 3-mercapto-1,2-propanediol, to name just a few. However, in the present work, we focus on a novel "striped" amphiphilic ligand shell first described by the laboratory of Francesco Stellacci [29]. A "striped" gold nanoparticle has unique mixture of hydrophilic (11-mercaptoundecane sulfonate, MUS) and hydrophobic (octanethiol, OT) ligands on its surface. In early studies, Stellacci and colleagues discovered that striped NPs exhibit unusual solubility properties mediated by the variation in hydrophilic and hydrophobic moieties organized over nanometer length scales on the particle surfaces [29].

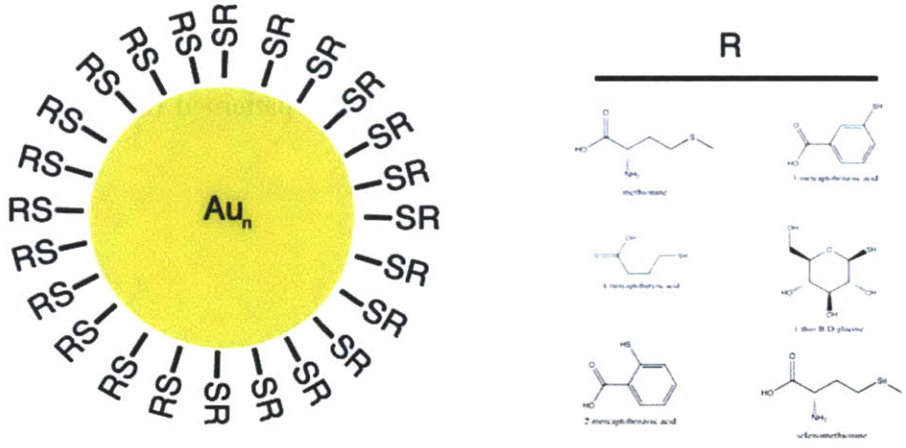

Figure 1-1: Water-soluble monolayer-protected gold clusters (MPCs) have been an object of investigation by many research groups since their first syntheses were reported in 1998 and 1999 [6].

Shells comprised of alternating hydrophobic and hydrophilic ligands are described as "striped" patterns in this work. Striped pattern formation is due to spontaneous phase separation of mixed ligands, and

domain ordering is sensitive to particle size, curvature, ligand length and composition. Self-assembled submolecular striped patterns were shown by simulation results to be entropy-mediated (Figure 1-2) [42]. Mixed short/long hydrophobic/hydrophilic ligands self assembled into microscopic phase-separated shells, whereas same length ligands self assemble into macroscopic phase-separated shells. Long ligands in a striped configuration possess larger free volume maximizing the surface's entropy capacity (a.k.a. "entropy favorable" pattern determination). The combination of long-range electrostatic repulsion and short-range enthalpic attraction led to the observed "striped" pattern as opposed to "checkerboard" patterns.

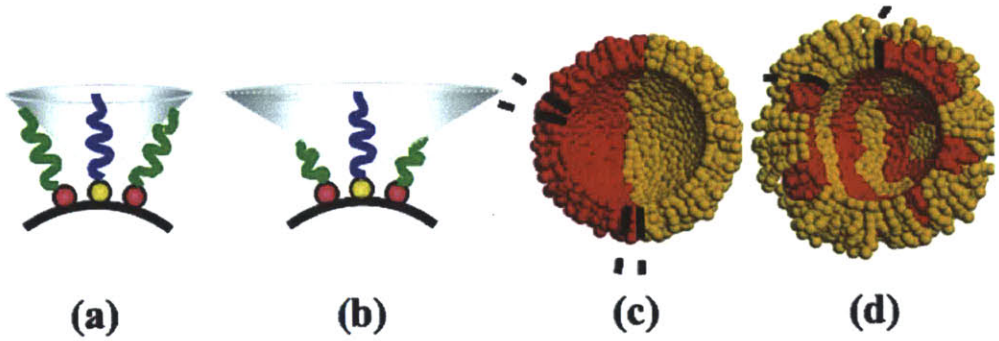

Figure 1-2: (a),(b) Schematic two-dimensional representation of shared free volume (conical shaded area) available to surfactant tails when they are surrounded by other surfactants on curved surfaces, for equal-length and unequal-length surfactants, respectively [42].

Strikingly, Verma et al. found that these striped gold particles can penetrate live cells through energy independent non-endocytic pathways—however homogeneous patterned (all MUS) gold nanoparticles cannot (Figure 1-3) [45].

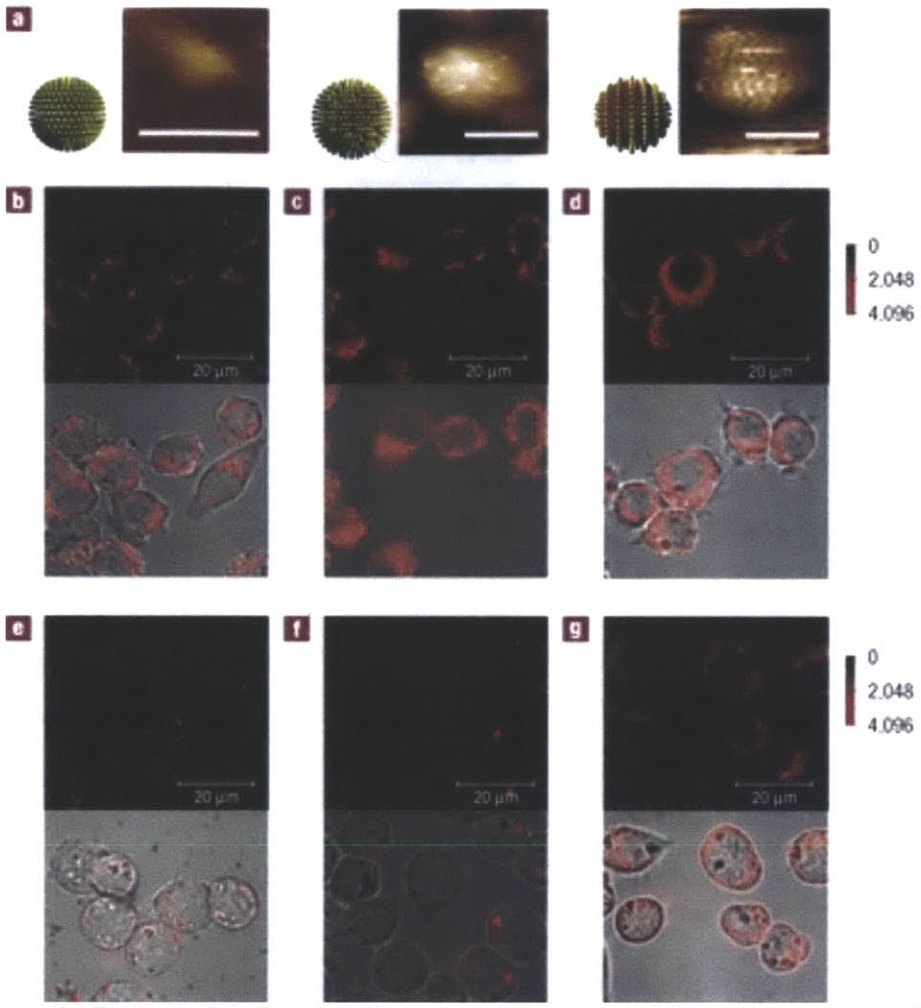

Figure 1-3: **a**, Schematic diagrams of the ligand shell structure of the nanoparticles and representative STM images (scale bars 5 nm). **b–g**, BODIPY fluorescence (upper panels with an intensity scale bar (a.u.)) and bright field/fluorescence overlay (lower panels) images of dendritic cells incubated with 0.2 mg ml^{-1} of MUS (**b**,**e**), 66-34 br-OT (**c**,**f**) or 66-34 OT (**d**,**g**) nanoparticles for 3 h in serum-free medium at 37 °C (**b–d**) or 4 °C (**e–g**). Image adapted from reference [45].

The mechanism of membrane penetration is under investigation in our lab. A "Membrane embedding" hypothesis was proposed and simulated by Van Lehn et al. and suggested that ligands on the gold surface are environmentally responsive, with hydrophobic tails capable of displaying in certain directions to minimize the surface energy of the whole system. The free energy of membrane embedding is dependent on the hydrodynamic size of gold nanoparticles, with 4.5 nm in diameter being the lowest (Figure1-4).

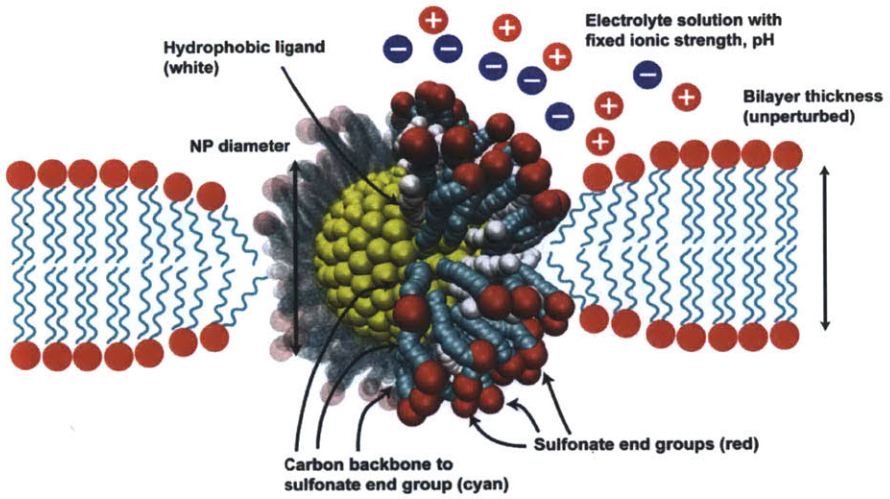

Figure 1-4: Simulation result of flexible environmental responsive ligands of MUS:OT gold nanoparticles (Reid Van Lehn and Alfredo Alexander-Katz, personal communication).

Jewell et al. demonstrated that striped gold nanoparticles facilitate intracellular oligonucleotide delivery, bypassing endocytic delivery barriers. DNA conjugated on striped NPs (MUS:OT 1:1) entered cells efficiently even when endocytosis was blocked with pharmacological inhibitors [26].

MUS:OT 1:1 gold nanoparticles also facilitate delivery of other membrane-impermeable biological macromolecules. Protein surface decoration with striped gold nanoparticles may mediate cell membrane penetration, leading to a potential means to cross hurdles of the delivery of large molecules, and is completely different from conjugation of macromolecules using gold nanoparticles as a ligand to achieve the same end.

1.3 Introduction to Interbilayer-Crosslinked Multilamellar Vesicles (ICMVs)

Notably, the results described above for interactions of striped NPs with the lipid membranes of living cells also apply to the interactions of striped NPs with synthetic membranes. Based on the findings described above, we hypothesize that lipid vesicles resistant to non-specific protein binding, infused with membrane-embedded gold nanoparticles, may enhance *in vivo* gold nanoparticle delivery to targeted tissue sites such as tumors. Such lipid vesicles containing pharmaceuticals in addition to gold nanoparticles may enable co-delivery of gold nanoparticles and the pharmaceutical agent(s) for clinical treatment of cancer via simultaneous radio- and chemotherapy.

A promising candidate vesicle system for attempting such striped NP delivery is based on interbilayer-crosslinked multilamellar vesicles (ICMVs), a multilayer lipid nanocapsule recently developed in our laboratory [35]. Moon et. al. introduced divalent cations to fuse anionic maleimide functionalized liposomes, and then covalent crosslinks between functionalized lipid headgroups of adjacent opposed bilayers using dithiothreitol (DTT) within preformed multilamellar vesicles (MLVs) to form ICMVs (Figure 1-5). Post PEGylation blocked uncapped maleimide headgroups and inhibited vesicles fusion. PEGylated ICMVs were stable in 4 °C for more than a week. ICMVs loaded with protein retain biodegradability while increasing protein retention in the presence of serum.

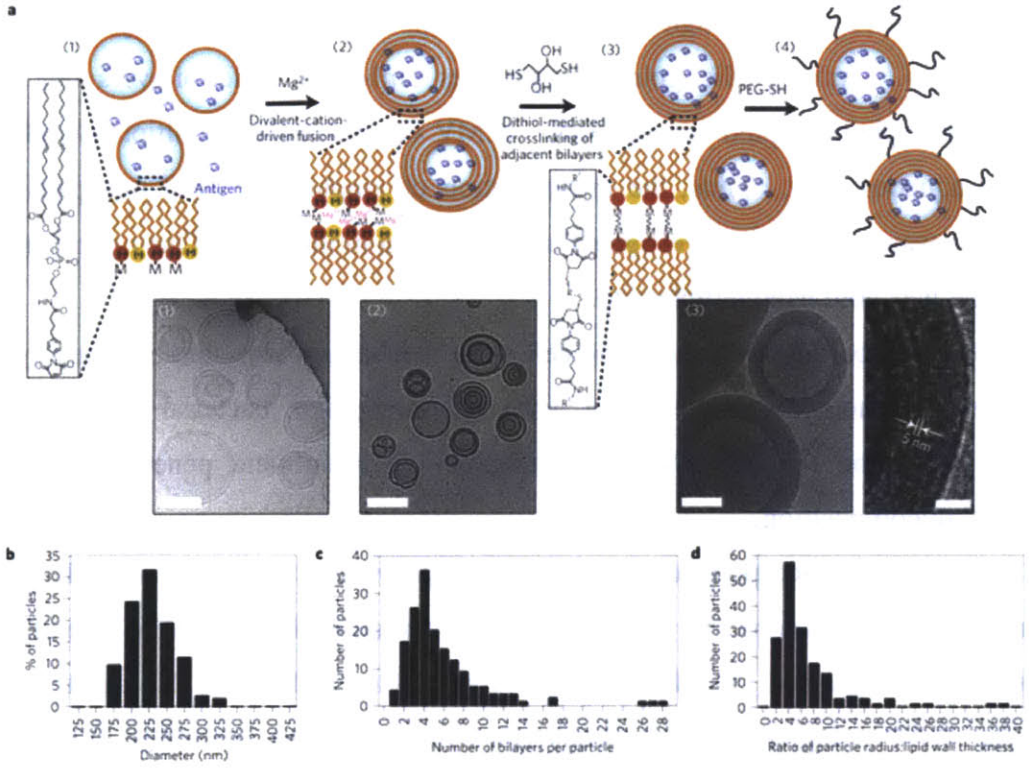

Figure 1-5: a, Schematic illustration of ICMV synthesis and cryo-electron-microscope images: (1) anionic, maleimide-functionalized liposomes are prepared from dried lipid films, (2) divalent cations are added to induce fusion of liposomes and the formation of MLVs, (3) membrane-permeable dithiols are added, which crosslink maleimide lipids on apposed lipid bilayers in the vesicle walls, and (4) the resulting lipid particles are PEGylated with thiol-terminated PEG. Cryo-electron-microscope images from each step of the synthesis show (1) initial liposomes, (2) MLVs and (3) ICMVs with thick lipid walls. Scale bars=100 nm. The right-hand image of (3) shows a zoomed image of an ICMV wall, where stacked bilayers are resolved as electron-dense striations; scale bar=20 nm. b, ICMV particle-size histogram measured by dynamic light scattering. c,d, Histograms of ICMV properties from cryo-electron-microscope images show the number of lipid bilayers per particle (c) and the ratio of particle radius to lipid wall thickness (d). (n=165 particles analyzed.) [Figure adapted from reference [35].

The number of lipid bilayers increases the average density of ICMVs resulting in increased centrifugal separation efficiency. This is essential for the development of clinical applications of gold nanoparticle decorated ICMVs and pharmaceutical bearing ICMVs, as discussed in greater detail in chapter 3.

1.4 Scope of Thesis

The scope of this thesis is the design and application of amphiphilic gold nanoparticle-decorated lipid vesicles to prospective clinical treatments. To support this, the mechanisms of interaction between amphiphilic gold nanoparticles and lipid membranes are also investigated.

The first objective is the design of suitable vectors for selective delivery of amphiphilic gold nanoparticles *in vivo*. Amphiphilic gold nanoparticles embed in lipid bilayers due to its unique hydrophilic and hydrophobic ligand arrangement. ICMV vectors provide multiple closely packed lipid bilayers and an aqueous core. Thus, the incorporation of amphiphilic gold nanoparticles into lipid bilayers in ICMVs was extensively investigated and optimized in this work. One optimization parameter of primary interest was gold nanoparticle size.

The striped nanoparticle non-endocytic cell entry mechanism was studied using synthetic model cell membranes. Nanoparticle interaction with gram-negative bacterial membranes was also investigated to determine the dependence of nanoparticle membrane penetration ability on lipid membrane structure/composition.

Gold nanoparticles incorporated in ICMVs may provide a better way to deliver concentrated gold nanoparticles *in vivo*. In order to accomplish this, interactions between ICMVs and non-target cell membranes must be suppressed. Gold nanoparticles embedded in ICMVs also must not interact with non-target cells. ICMVs degraded endocytically allow the membrane interactive gold nanoparticles to freely distribute into intracellular membranes of targeted cells. Synthetic lipid membranes were investigated as a means to these ends. Experiments testing whether gold nanoparticles on PEG protected ICMV migrate from their original bilayer to neighboring model cell membrane were conducted.

The final subject of investigation was gold nanoparticles' effect on radiotherapy-mediated cell membrane disruption and genome damage, to evaluate the potential of this approach to enhance local radiation therapy of cancer, and minimize side effects on peripheral normal tissues (Figure 1-6). We hypothesize that the intracellular location of radiosensitizers may localize damage to specific cellular

compartments. Thus, cellular uptake of gold nanoparticle-decorated ICMVs was studied to evaluate uptake efficacy and intracellular migration capability.

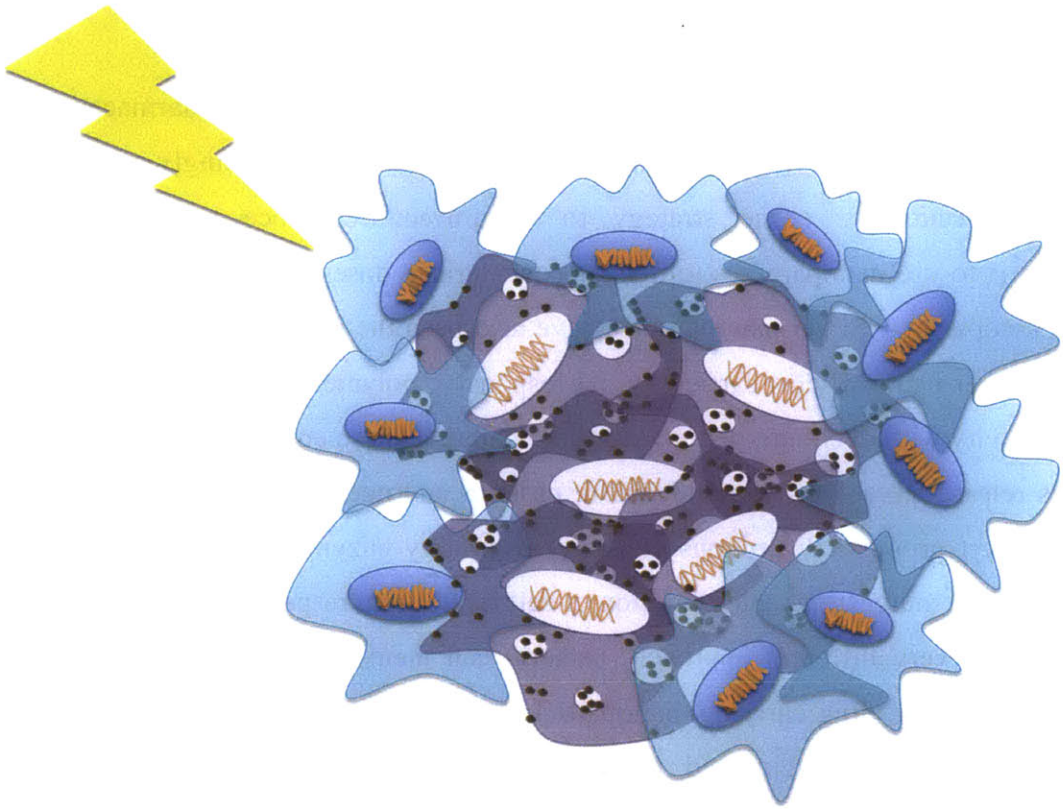

Figure 1-6: Gold nanoparticle selectively loaded in tumor cells (purple) but not the peripheral healthy cells (blue).

2 Attachment of Amphiphilic Gold Nanoparticles to Bacteria

2.1 Introduction

Since the development of antibiotics, improper administration of antibiotic pharmaceuticals has been a powerful selective pressure driving the evolution of bacteria that are increasingly resistant to established antibiotic pharmaceuticals. One strategy to circumvent resistance to conventional treatment methodologies is to use nanoparticles to deliver concentrated doses of existing antibiotics directly into the bacterial cytoplasm. Silver nanoparticles have also been the subject of extensive investigation [1]. For example, silver nanoparticles carried by pH responsive polymers are effective in mitigating partial loss of drug activity with declining pH *in vitro* [46]. Subsequent to entry into bacterial cytoplasm, silver nanoparticles release silver ions which denature proteins and nucleic acids via combination with thiol, carboxyl, hydroxyl groups. Silver ions denature respiratory enzymes, proteases, and bind with DNA causing suffocation, indigestion, and inhibition of cell replication, respectively.

In another very different approach, bacteria can themselves be envisioned as drug delivery chaperones, by linking drug-carrying nanoparticles to tumor-homing microbes (Figure 2-1). For example, bacteria can be engineered to deliver plasmid DNA coated nanoparticles in clinical applications such as vaccination and cancer therapy [40]. Transfection of plasmid DNA requires bacterial degradation prior to release, whereas nanoparticle vectors deliver plasmid DNAs directly to the intracellular milieu.

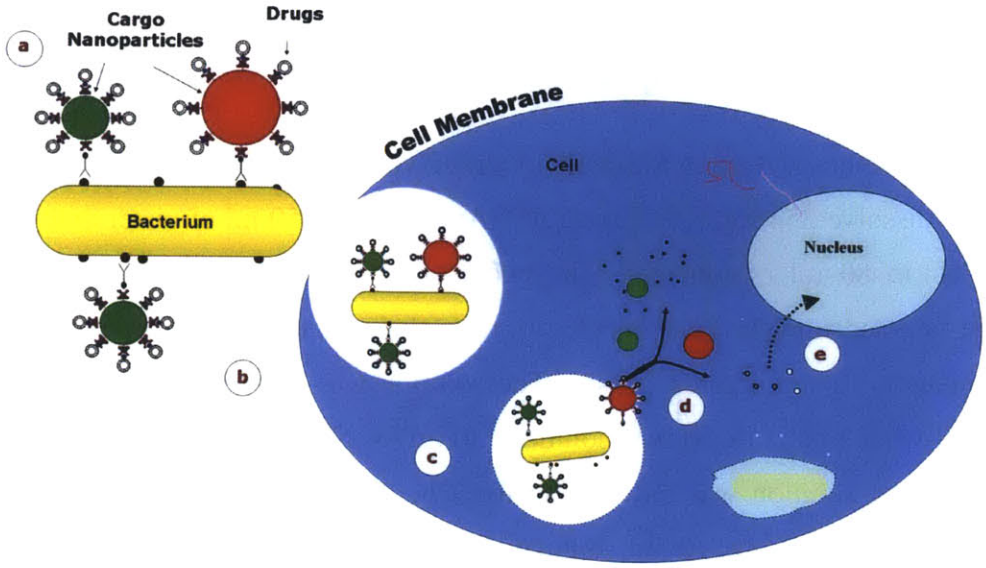

Figure 2-1: Delivery begins with a) cargo carrying bacteria that are b) engulfed by the receiving cell. The bacterium then c) dissolves the endocytic membrane and d) releases its contents which may also be e) sent to the nucleus. Illustration adapted from [1].

Motivated by these potential applications, our aim was to attach striped gold nanoparticles to bacterial membranes. Nanoparticles that carry drugs can serve as antibiotic vectors and concentrate drugs to the vicinity of bacterial membranes, thus minimizing side effects and enhancing killing efficiency. Hydrophobic drugs that may otherwise be undeliverable can be carried with amphiphilic nanoparticles by adsorbing into hydrophobic pockets (Figure 2-2) [31], while hydrophilic drugs can be directly conjugated to gold nanoparticles by modification of thiol-terminated chemical linkers on potential drugs.

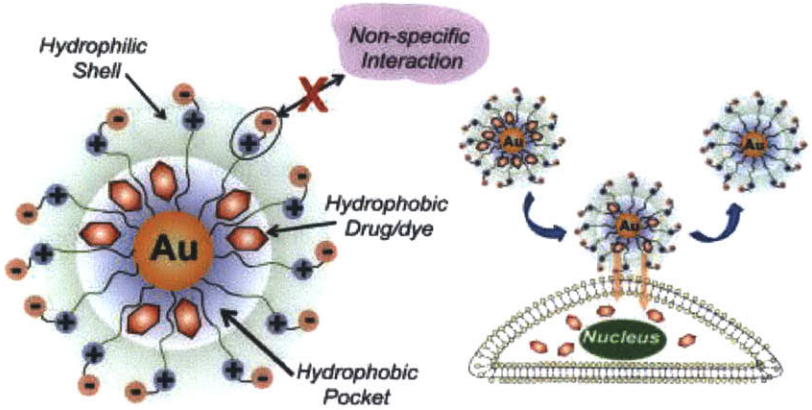

Figure 2-2: Gold nanoparticles functionalized with water-soluble zwitterionic ligands form kinetically stable complexes with hydrophobic drugs and dyes. Illustration adapted from reference [31].

2.2 Experimental Methods

2.2.1 Synthesis of Striped Gold Nanoparticles

Nanoparticles were synthesized using a slightly modified version of the Schriffin method. The general procedure was to dissolve 354 mg (0.9 mmol) of $HAuCl_4 3H_2O$ in 50 ml of water and 2.187 g (4 mmol) of $BrN((CH_2)_7CH_3)_4$ in 80 ml of toluene. The two phases were mixed and left stirring for 30 min. Mixtures of the targeted ligands were injected in the solution once the color due to the gold salt had transferred completely to the organic phase. The solution was allowed to react for ten minutes and acquired a typical white color. A 10 mM solution (30 ml) of $NaBH_4$ was then added dropwise over 1 h. After the addition, the solution was left stirring for 2 h. The phases were separated and the organic phase was collected, reduced to 10 ml, diluted with 100 ml of absolute ethanol, and placed in a refrigerator overnight. The precipitate was collected by vacuum filtration using quantitative paper filters and extensively washed with water, acetone (Method adapted from reference [29]). MUS:OT 1:1 nanoparticle cores in this study were either 2.18 ± 0.47 nm or 4.2 ± 0.5nm (Figure 2-3 and 2-4) in diameter.

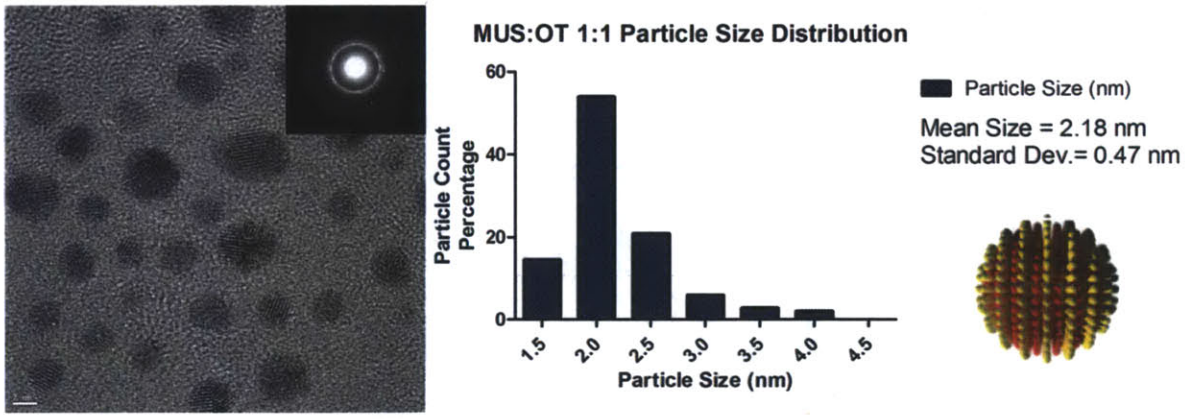

Figure 2-3: TEM image of MUS:OT 1:1 and size distribution of the nanoparticles.

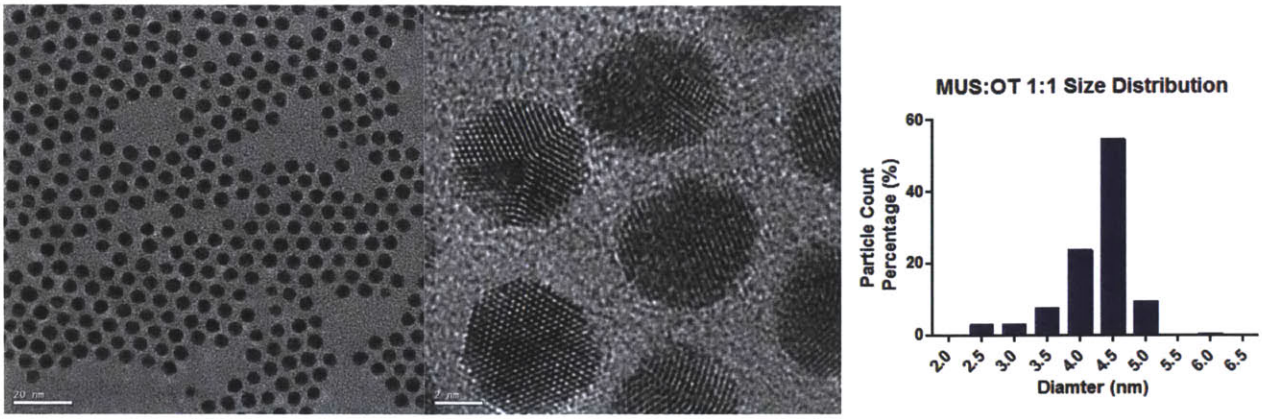

Figure 2-4: TEM image of MUS:OT 1:1 gold nanoparticles of lager size.

2.2.2 TEM Sample Preparation for Thin-Sectioned Biological Samples

Thin-sectioned electron microscopy was conducted to more precisely determine the location of the amphiphilic gold nanoparticles in or on affected cells. After 5 hours of incubation of of 0.6 mg/mL 1:1 MUS:OT gold nanoparticles with *E. Coli* (5 million cells/mL) in the presence of antibiotics (cefotaxime) at 37°C, the cells were washed 2X with phosphate-buffered saline pH 7.4 (PBS) to remove unbound nanoparticles. The cells were fixed in 2.5% gluteraldehyde, 3% paraformaldehyde with 5% sucrose in 0.1M sodium cacodylate buffer (pH 7.4) for 1 hr at 4°C, pelleted, and post fixed in 1% OsO_4 in veronal-acetate buffer. The cell pellet was stained in block overnight with 0.5% uranyl acetate in veronal-acetate buffer (pH 6.0), then dehydrated and embedded in Embed-812 resin. Sections were cut on a Reichert Ultracut E microtome with a Diatome diamond knife at a thickness setting of 50 nm, stained with uranyl acetate, and lead citrate. Thin-sectioned sample grids were prepared by Nicki Watson in the Whitehead Institute.

2.2.3 Fluorescent Dye Labeling of Gold Nanoparticles

To track gold nanoparticles under fluorescent microscopy, they were labeled with BODIPY-SH (Figure 2-5). The procedure is described here. 5 μL of BODIPY-SH (2.45 mg/ml in 2:1 water: dimethylformamide mixture) was added to 10 mg of gold nanoparticles in water ; the final gold nanoparticle concentration was kept at 10 mg/ml. The solution was covered with foil to protect it from light and agitated at speed of 750 rpm on a shaker for 3-4 days at 25°C. Unconjugated BODIPY-SH

was completely removed by topping up the eppendorf with acetone and centrifuging at 14 kxg for 2 minutes (repeated four times). Excess acetone was evaporated in the vacuum oven overnight. Finally, solubilize dried nanoparticles in a desired solution and calculate the nanoparticle concentration by reading the absorbance at 520 nm.

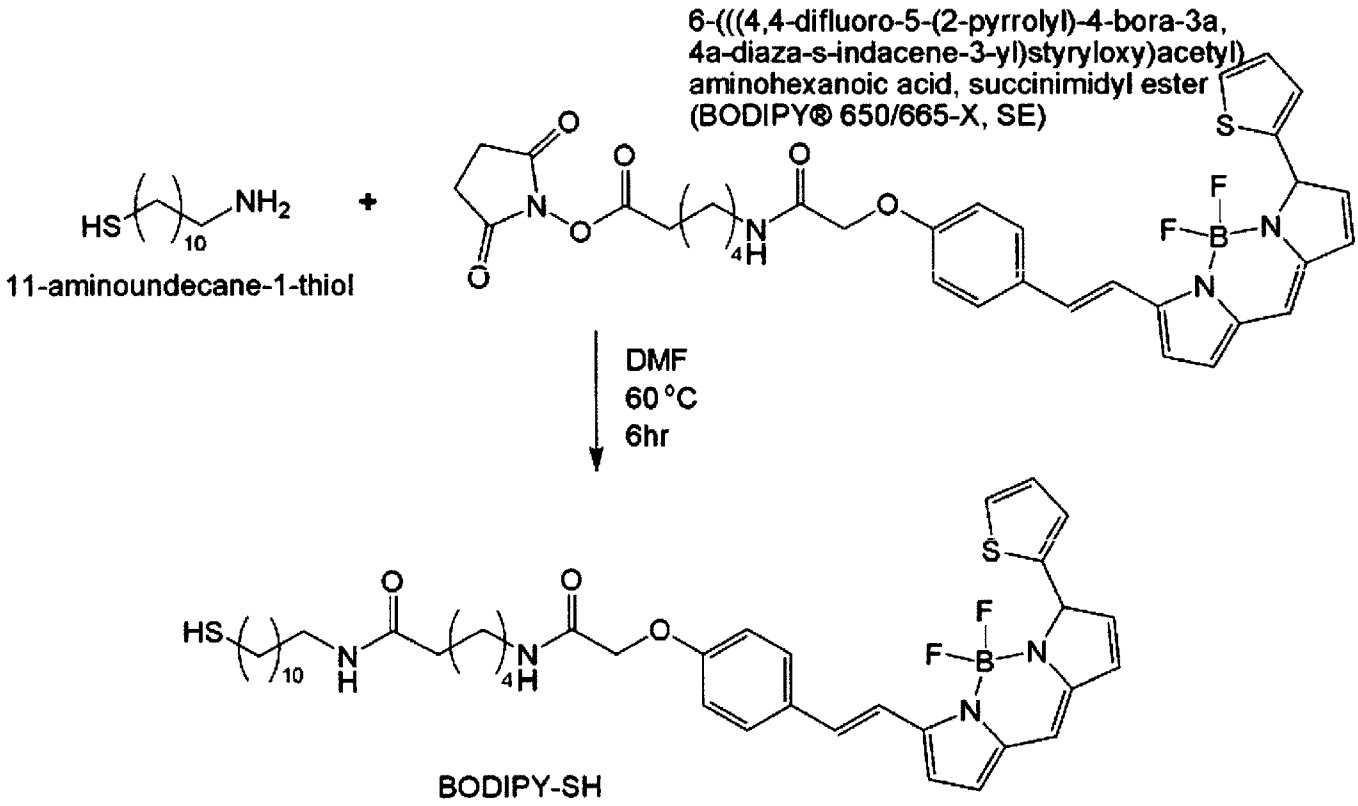

Figure 2-5: 11-aminoundecane-1-thiol purchased from Prochimia (Poland) (0.93 mg, 4.6 μmol) was reacted with 6-(((4,4-difluoro-5-(2-pyrrolyl)-4-bora-3a,4a-diaza-s-indacene3yl)styryloxy)acetyl) aminohexanoic acid, succinimidyl ester (BODIPY® 650/665-X, SE) purchased from Invitrogen (California, USA), (2.7 mg, 4.2 μmol) in 1 mL of DMF at 60 °C for 6 h under inert atmosphere. Illustration adapted from reference [45].

2.3 Results and Discussion

2.3.1 Using Red Blood Cells as a sensor for Dye conjugation

Striped nanoparticles have been observed to penetrate all mammalian cell membranes tested—except red blood cell membranes. While the cause of these results is not fully understood, it has been observed

that the glycocaylx of RBCs may play an important role in blocking nanoparticles interaction with membranes.

Figure 2-6 shows that free alkanethiol-bodipy dye effectively labeled RBC cell membranes, however, dye labeled nanoparticles did not interact with RBC membranes at all. Future work may utilize this result by using RBCs as sensors as a dye conjugation test; if there was excess bodipy dye adsorbed in the hydrophobic pockets of gold monolayers (as opposed to covalently bonded via thiol group to the gold surface), it would have transferred to the RBC membranes. We observed that dye-labeled particles did not interact with the RBCs. This implies that no free dye was adsorbed in the hydrophobic layer of gold nanoparticles, therefore the observed fluorescent signals came from dye-conjugated nanoparticles—not free dye. Notice that red blood cells were "spiky" because of the hypertonic PBS environment which caused membrane shrinkage. However, this does not affect our result.

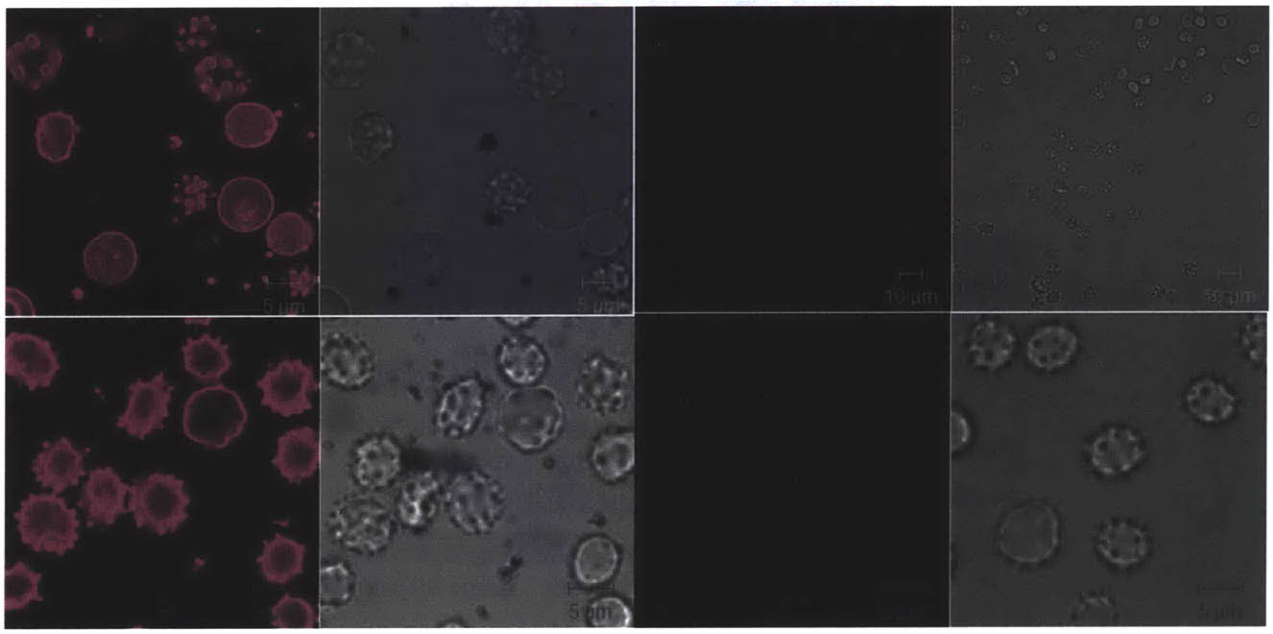

Figure 2-6: Free dye transferred on RBC membrane at both 37°C (upper left) and 4°C (lower left). Dye gold nanoparticles did not interact with RBC membranes at either temperature (right).

2.3.2 Adsorption of Gold Nanoparticles on Bacterial Cell Walls

2.3.2.1 Gold Nanoparticles interacting with Escherichia coli membranes

Bacterial cell walls consist of several membranes: an LPS outer membrane (only for gram-negative bacteria), peptidoglycan, and phospholipid inner membrane (Figure 2-7). It is known that most gram-negative bacteria cell walls contain gaps of 2-4 nm in the peptidoglycan layers, which block the entrance of most molecules. However, during cell division the cell wall synthesis process may provide an opportunity for the penetration of nanoparticles. Another alternative for aiding nanoparticle penetration may be to prevent cell wall division by addition of antibiotics. In this case, cells will elongate due to the inhibition of cell wall division, yielding a thinner cell wall that may contain defects facilitating nanoparticle attachment or penetration.

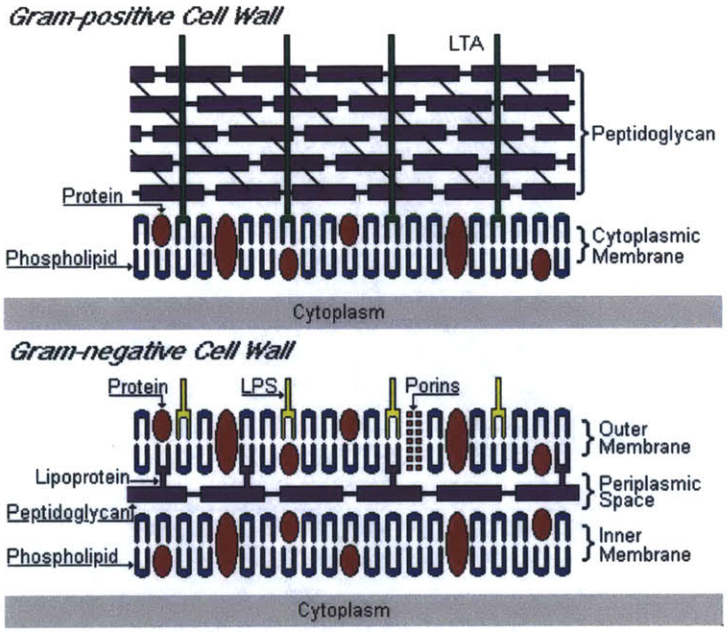

Figure 2-7: Gram-positive and gram-negative cell wall structures. Image adapted from *©1997-2013 Douglas F. Fix.*

To start our first experiment investigating amphiphilic gold nanoparticle attachment or penetration of bacterial cell walls, amphiphilic gold nanoparticles were incubated with gram-negative bacteria *E. Coli.* (transduced with GFP, provided by the Lu Lab at MIT) for five hours at 37°C. In the absence of antibiotics, interestingly, striped NPs were found to accumulate on the surfaces of bacteria but did not penetrate their cytosol. At the highest concentration of antibiotics addition, gold nanoparticles were observed to be co-localized with the *E. Coli.* However, due to lack of confocal microscopy resolution there is uncertainty as to whether or not this implies penetration of gold nanoparticles through *E. Coli.*

cell walls into the bacteria cytosols (lower panel in Fig. 2-8). The addition of antibiotics induced bacterial elongation, implying that cell wall synthesis had been effectively inhibited. Cells treated with antibiotics were also observed to be co-localized with gold nanoparticles. However, again, lack of confocal microscopic resolution introduces uncertainty as to whether or not the gold nanoparticles penetrated and resided in the bacterial membranes. Controls without antibiotics showed no penetration of nanoparticles but perhaps attachment on the cells' outer surfaces.

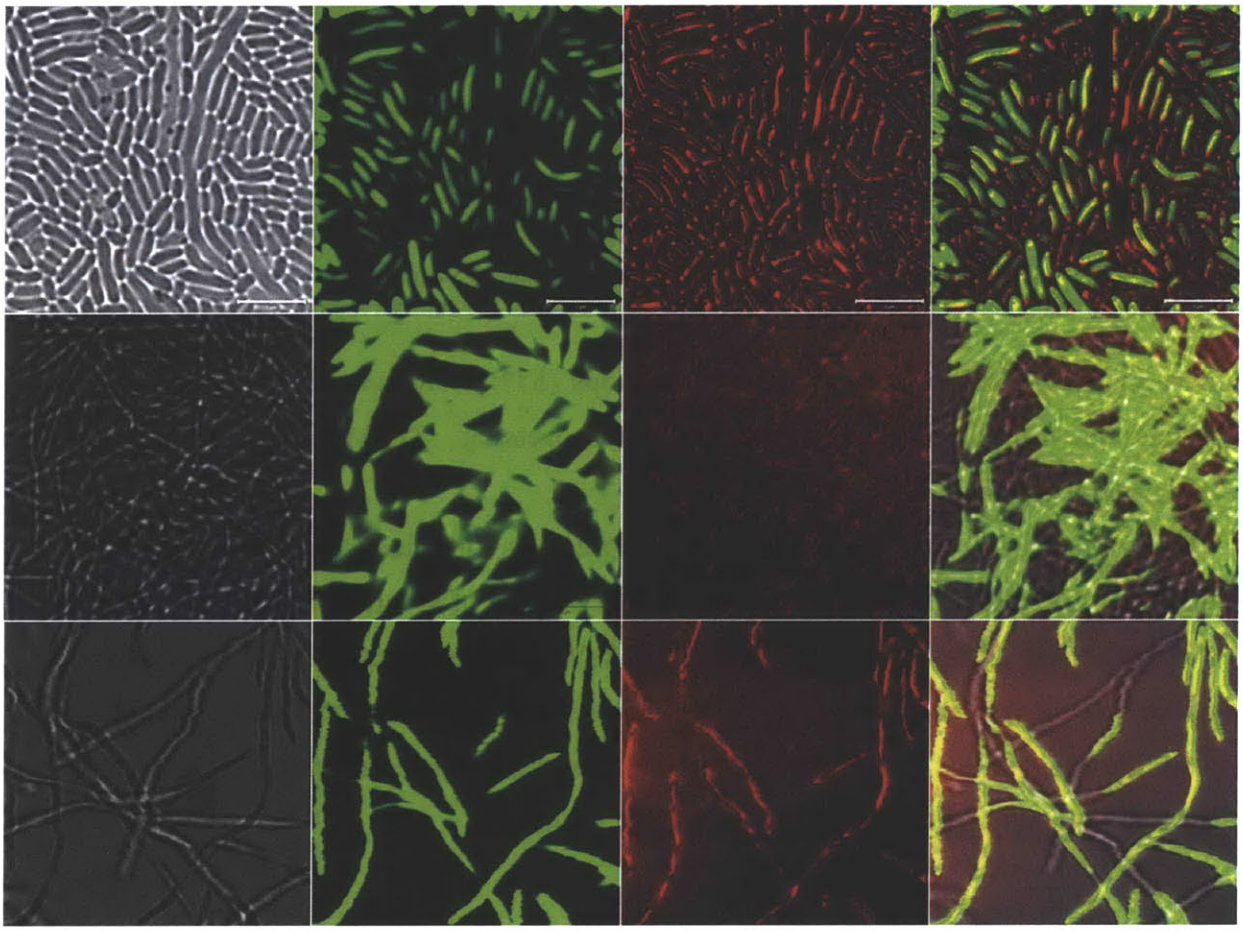

Figure 2-8: 5 hours of incubation with 0.2 mg/ml gold nanoparticles in LB medium (upper panel) at 37° C; 5 hours of incubation with gold nanoparticles and addition of 0.06uL of antibiotics (middle panel) or 0.6uL of cefotaxime. (Courtesy of P. Atukorale and S. Lemire)

Thin-sectioned TEM work was conducted for a better resolution imaging, however, most of the nanoparticles were unable to be visualized via TEM imaging due to the small size of nanoparticles and the heavy metal stain (Fig. 2-9).

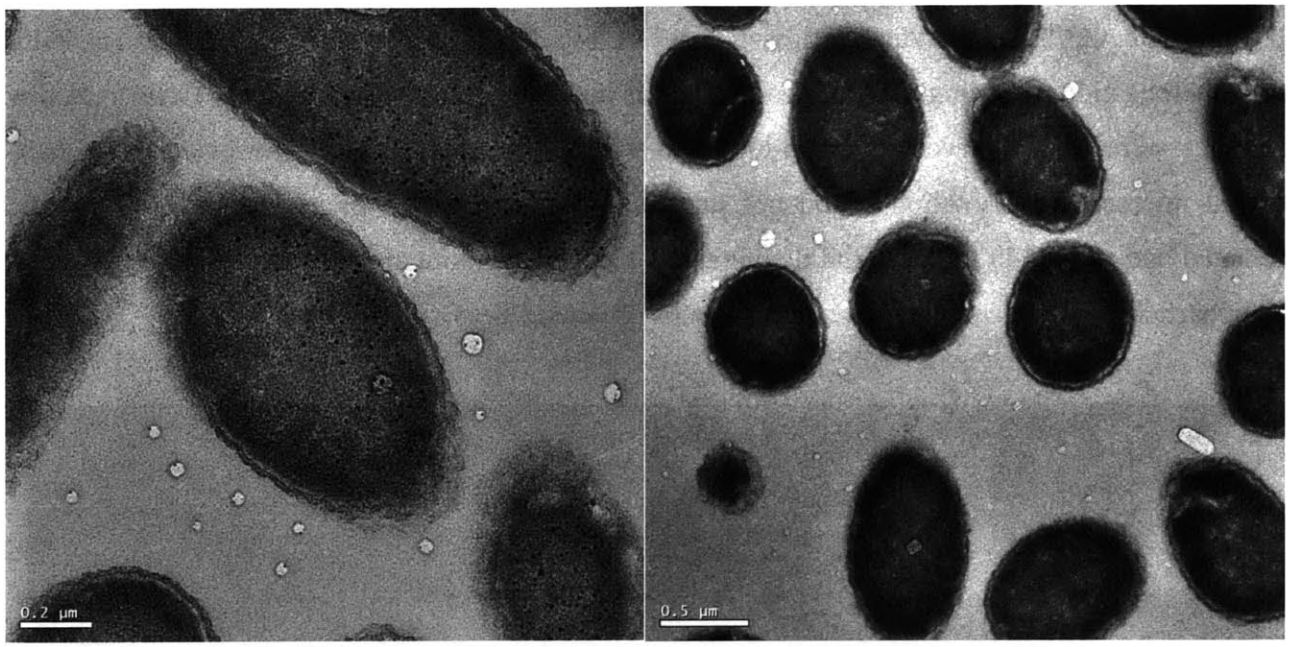

Figure 2-9: TEM image of thin-sectioned *E. Coli.* Gold nanoparticles of 5-7nm were observed inside the cells (left). However, most cells were stained by heavy metals and blocked the contrast of gold nanoparticles (right).

Z-contrast Scanning Transmission Electron Microscopy (STEM) microscopy was unable to image gold nanoparticles on the surface of heavy metal-stained bacteria. STEM image of gold nanoparticles decorated bacteria is shown in Figure 2-10.

Energy dispersive x-ray spectroscopy (EDS) detects and quantifies relative proportions of all elements above Li present in a given region, with a resolution of several nanometers. Au nanoparticles have a characteristic X-ray emission peak at 2.2 keV. The element map and spectrum (Fig 2-11) revealed that the main elements present in our samples were the uranium (green dots) and lead (blue dots) from the heavy metal stains. Few gold (red dots) signals detected via EDS, indicating that gold nanoparticles were not highly loaded on bacteria cell walls.

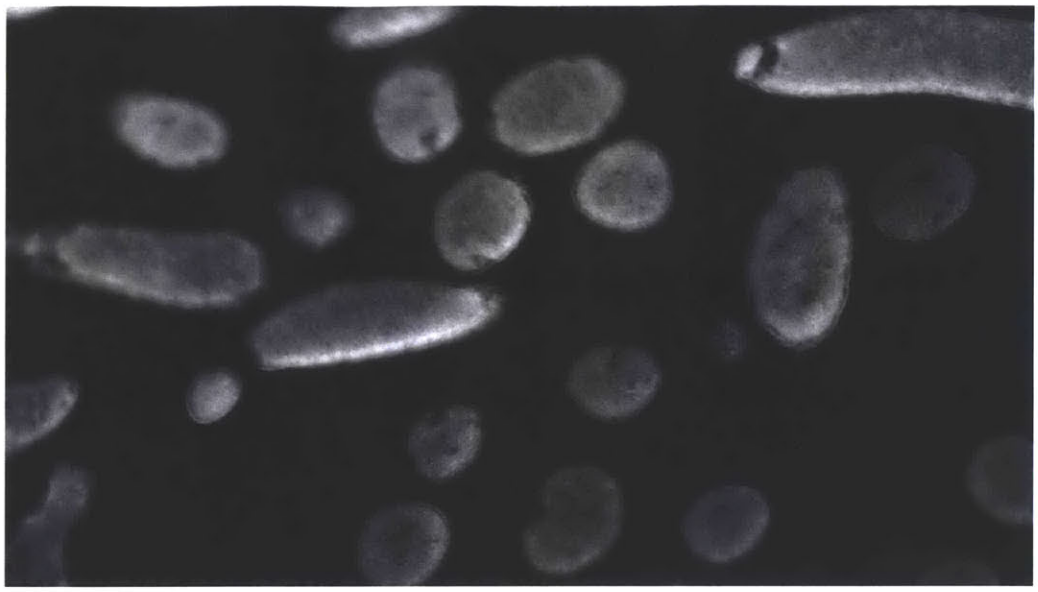

Figure 2-10: STEM image of thin-sectioned gold loaded *E. Coli*.

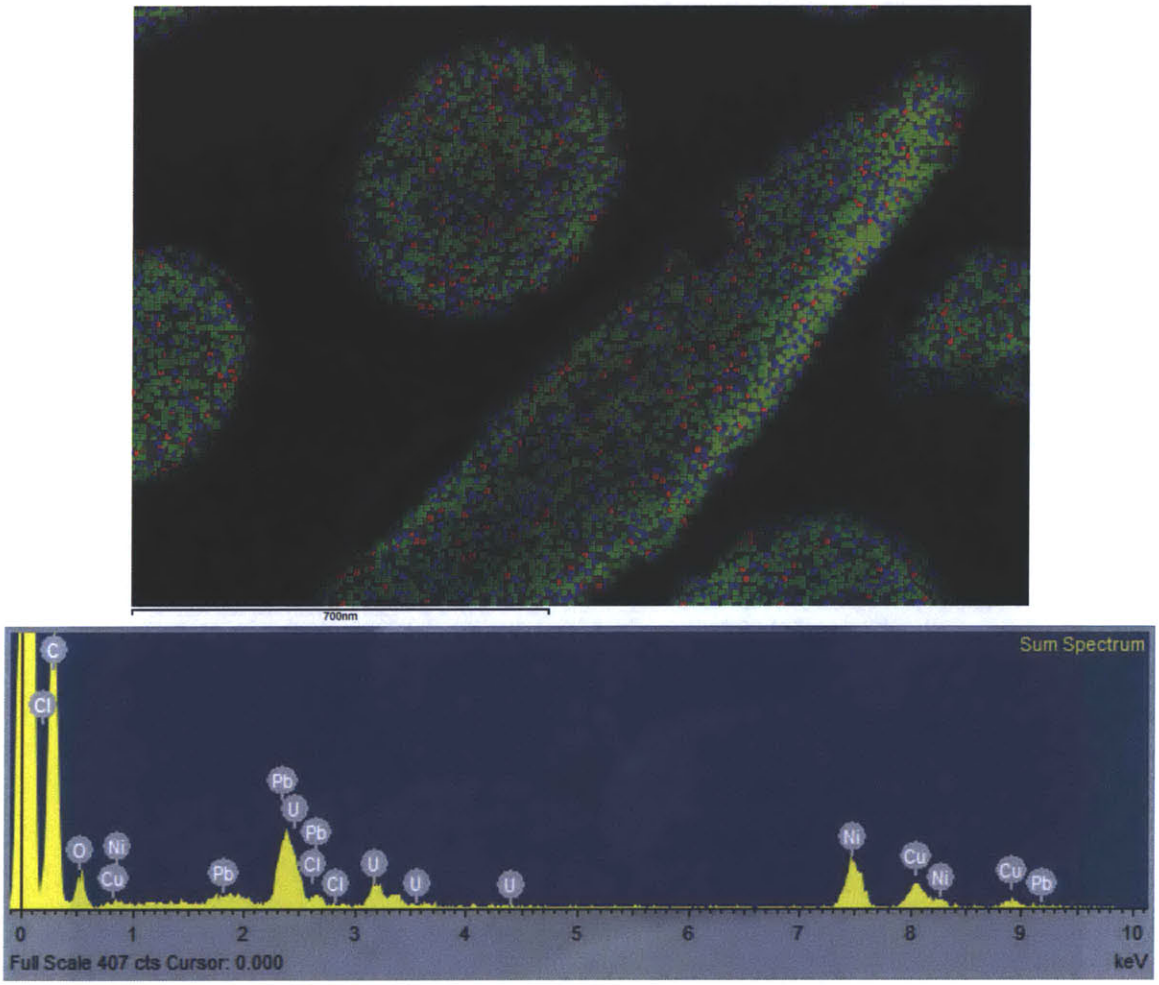

Figure 2-11: Elemental map (upper) and EDS spectrum (lower) of bacteria with gold nanoparticles.

2.3.2.2 Gold Nanoparticles on *Salmonella* membranes

Salmonella, another gram-negative bacterium, has the same cell wall structure as *E. Coli*. We observed that our membrane interactive gold nanoparticles attach to *Salmonella* cell walls. The kinetic study revealed that the attachment of gold nanoparticles on *E. Coli*. significantly increased at 24 hours of incubation. The degree of bacterial pellet darkening was proportional to the incubation time, ranging from a light violet at 6 hours to a dark purple at 24 hours.

In order to image the Salmonella and treated with gold nanoparticles, the uranyl acetate and lead citrate stainings were omitted. This method of visualization was successful, although image resolution was degraded. Gold nanoparticles incubated with Salmonella for 6 hours at 37 °C effectively attached to Salmonella cell walls without the treatment of antibiotics (Figure 2-12). Some bacteria appeared to bud out outer membrane vesicles (OMV) [47], forming membrane spheres decorated with gold nanoparticles (Figure 2-13).

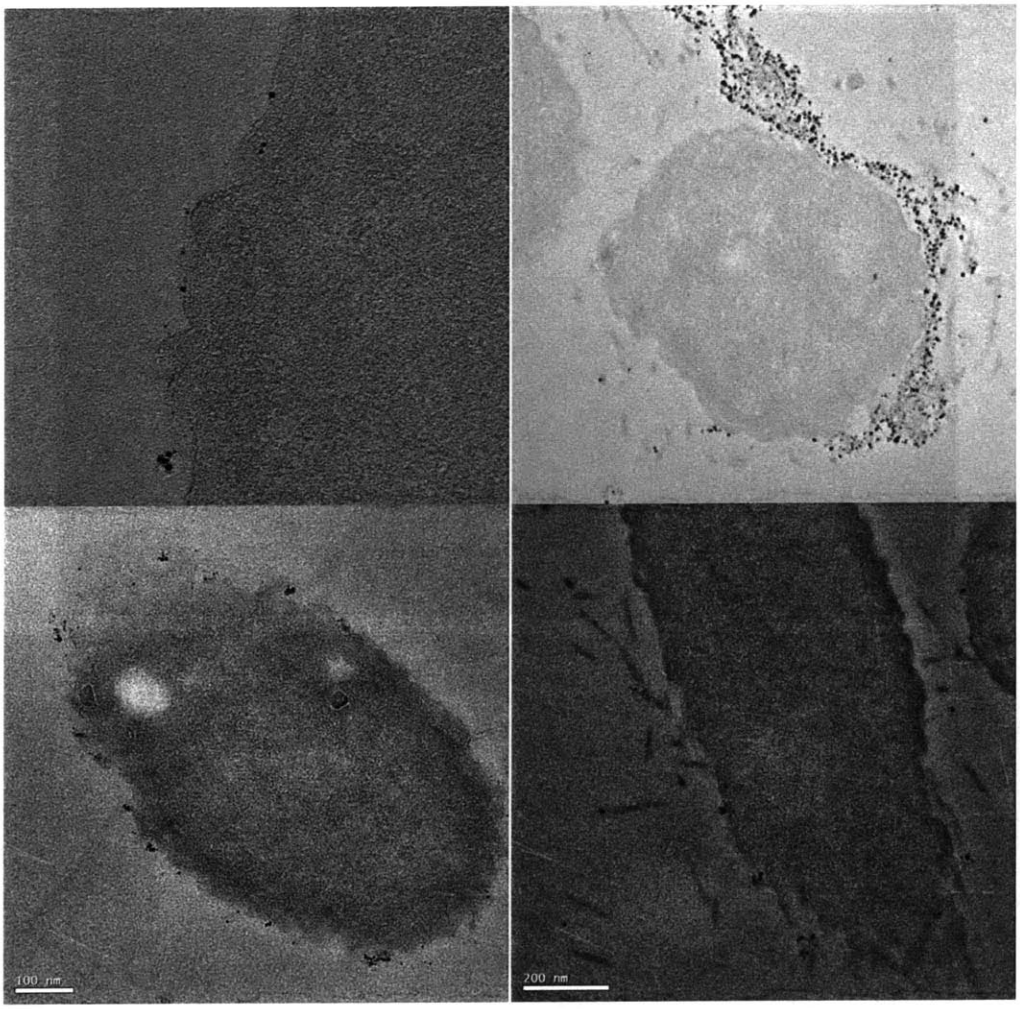

Figure 2-12: TEM image of thin-sectioned Salmonella with gold nanoparticles attached on their surface.

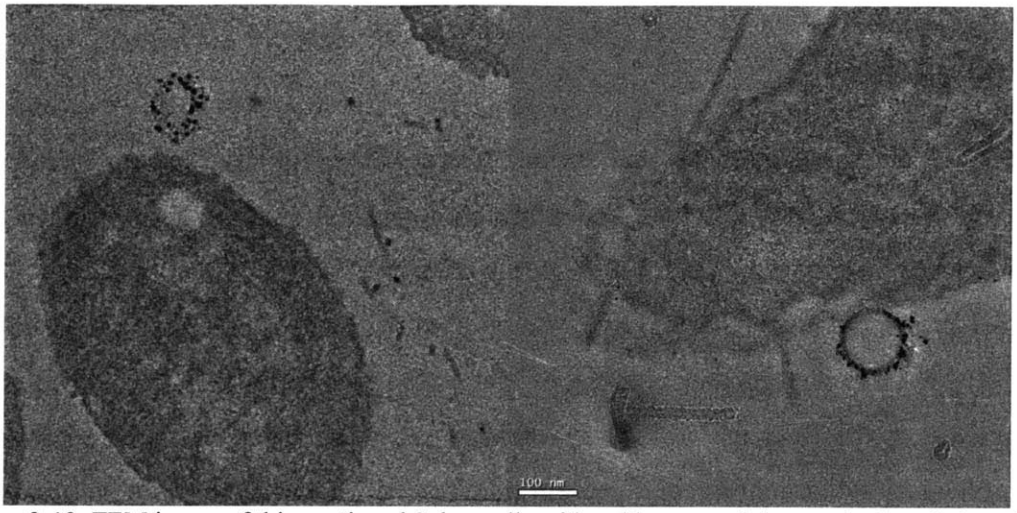

Figure 2-13: TEM image of thin-sectioned Salmonella with gold nanoparticles attached on their surface.

2.4 Conclusions

Amphiphilic gold nanoparticles have been observed to attach to the gram-negative bacterial membranes of both *E.Coli.* and *Salmonella.* Confocal imaging produced inconclusive results potentially implying nanoparticle attachment in the presence of antibiotics inhibiting cell wall synthesis. High resolution TEM images revealed that gold nanoparticles attached to both bacterial cell walls and were potentially blocked at the peptidoglycan layer which provided steric hindrance for the entry of nanoparticles, regardless of the presence or absence of antibiotics. Moreover, some bacteria are known to secrete fimbriae, and the amphiphilic gold nanoparticles attached to these materials. It was also observed that bacteria budded out membrane vesicles decorated with gold nanoparticles.

Gold nanoparticles were attached to gram-negative bacterial walls by incubation of cells with membrane-interactive amphiphilic gold nanoparticles at ambient conditions. The success of these results suggest that further work on loading hydrophobic drugs in hydrophobic pockets of amphiphilic gold nanoparticles for effective drug delivery to bacteria is warranted.

3 Design and Formation of Gold Nanoparticle-Decorated Lipid Vesicles

3.1 Background

Recent advances in chemical synthesis and surface functionalization have led to development of gold nanoparticles for biomedical applications, including photothermal ablation therapy [24], targeted drug and gene delivery [38], bioimaging [25], and radiation therapy [21].

Comprehensive *in vivo* studies have shown that biodistribution of nanoparticles is highly correlated with the size, charge and coating of the particles [30][3][2][37]. Particles of all sizes accumulate quickly in the liver and spleen and remain sequestered for extended periods [7][15][41]. One way to prolong blood circulation and prevent nonspecific protein adsorption is to introduce surface modification of PEG coatings on gold surface [32].

Unfortunately, *in vivo* studies have demonstrated that soluble gold nanoparticles are mostly retained in reticuloendothelial system (RES) and the amount of gold nanoparticles successfully delivered to tumor sites was relatively low. Long-circulating, pharmaceutical loaded liposomes have been an intensive subject of investigation. Researchers have demonstrated a thousand-fold enhancement in the cellular uptake of the small (1.4 nm) Au NPs into tumor cells *in vitro* by overcoming the energetically unfavorable endocytosis process for small NPs using liposomal delivery system [12]. Besides the advantage of prolonged blood circulation, liposomal surfaces can be modified by targeting ligands for specific applications. Figure 3-1 shows liposome-cell interactions, including passive diffusion and receptor-mediated endocytosis.

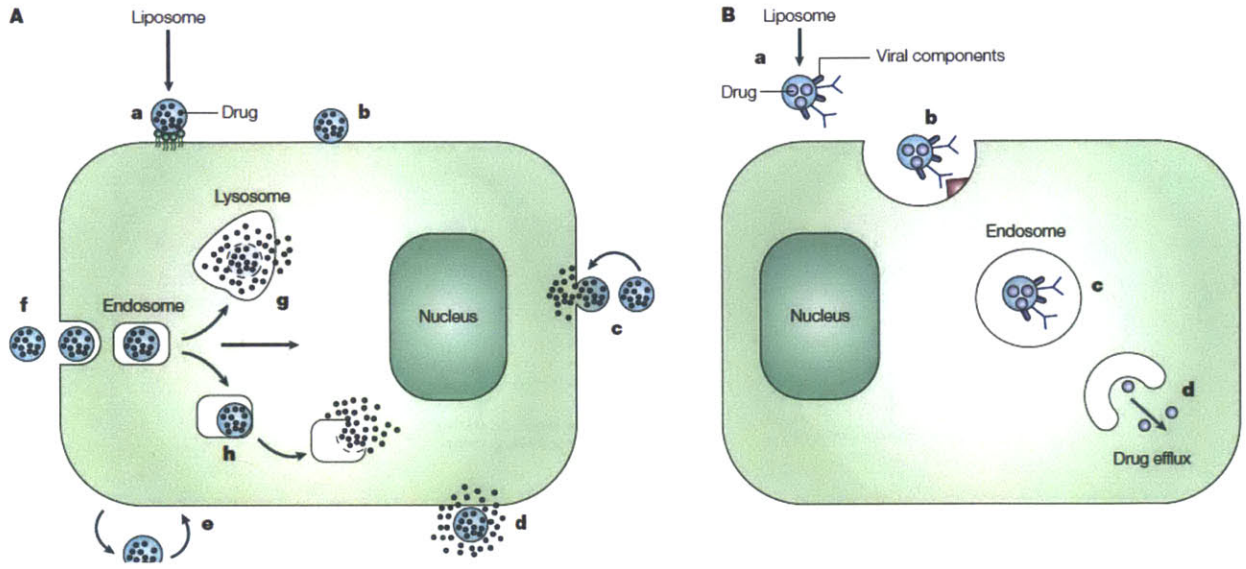

Figure 3-1: Figure 3 | Liposome-cell interaction. A | Drug-loaded liposomes can specifically (a) or nonspecifically (b) adsorb onto the cell surface. Liposomes can also fuse with the cell membrane (c), and release their contents into the cell cytoplasm, or can be destabilized by certain cell membrane components when adsorbed on the surface (d) so that the released drug can enter cell via micropinocytosis. Liposome can undergo the direct or transfer-protein-mediated exchange of lipid components with the cell membrane (e) or be subjected to a specific or nonspecific endocytosis (f). In the case of endocytosis, a liposome can be delivered by the endosome into the lysosome (g) or, en route to the lysosome, the liposome can provoke endosome destabilization (h), which results in drug liberation into the cell cytoplasm. B | Liposome modified with specific viral components (a) and loaded with a drug can specifically interact with cells (b), provoke endocytosis, and, via the interaction of viral components with the inner membrane of the endosome (c), allow for drug efflux into the cell cytoplasm (d). Illustration adapted from reference [44].

As discussed in chapter 2, MUS:OT 1:1 gold nanoparticles are known to be highly membrane interactive. Simulation results suggest that hydrophobic and hydrophilic ligands on nanoparticles are environmentally responsive. These results model flexible ligands reorganizing to lower the free energy of nanoparticles embedded in membranes. The embedding hypothesis showed that membrane penetration of nanoparticles was size and composition dependent (Van Lehn et al., unpublished result).

In this chapter, we describe efforts to generate "gold nanoparticle-decorated lipid vesicles" of 200nm size was designed as a gold nanoparticle delivery vector. The vesicles were post conjugated with PEG 2000 to provide prolonged circulation by inhibition of non-specific protein interactions— "stealth". Our aim is to improve cellular uptake of gold nanoparticles and control their targeting to tumors by the delivery of gold nanoparticle-decorated lipid vesicles instead of "free" gold nanoparticles, utilizing the enhanced permeability and retention effect (EPR effect [39]) for the extravasation of macromolecules (50-300nm) in solid tumor sites (Figure 3-2).

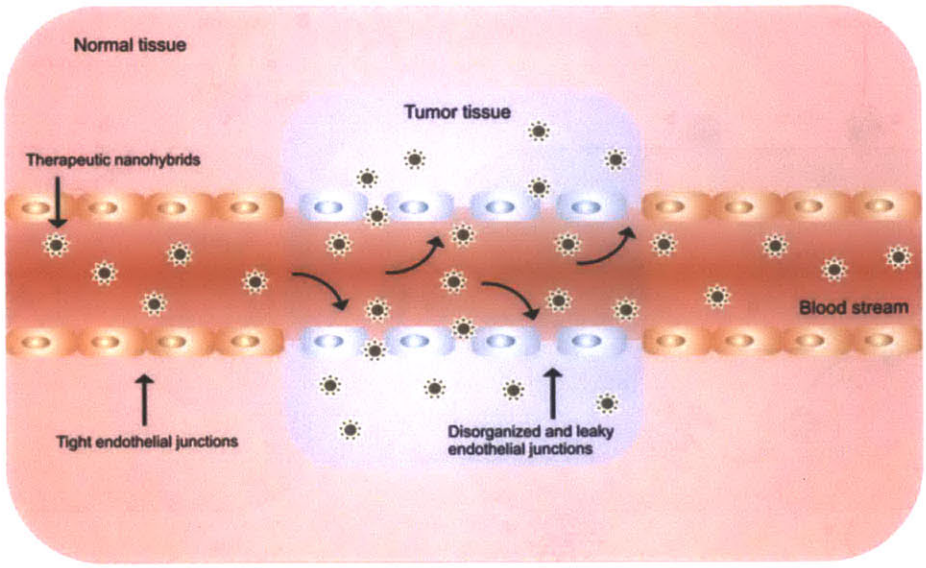

Figure 3-2: Schematic of tumor targeting by nanohybrids via Enhanced Permeation and Retention (EPR) effect [39].

3.2 Experimental Methods

3.2.1 Synthesis of Gold Nanoparticle-Decorated Lipid Vesicles

Synthesis of ICMVs [35]. 1.26 μmol of lipids in chloroform (typical lipid composition DOPC: MPB 1:1 molar ratio, all lipids from Avanti Polar Lipids, Alabaster, AL) were dispensed to glass vials, and the organic solvents were evaporated under vacuum overnight to prepare dried thin lipid films. The lipid films were rehydrated in 10mM bis-tris propane at pH 7.0 with cargo proteins for 1 h with rigorous vortexing every 10 min, and then sonicated in alternating power cycles of 6W and 3W in 30 s intervals for 5 min on ice (Misonix Microson XL probe tip sonicator, Farmingdale, NY). The liposomes formed in this first step were induced to undergo fusion by addition of divalent cations such as Ca^{2+} at a final concentration of 10 mM. The resulting MLVs were incubated with 1.5mM DTT (maleimide:DTT molar ratio of 2:1) for 1 h at 37 ^{O}C to conjugate opposing bilayers of maleimide-functionalized lipids and form crosslinked ICMVs; the resulting vesicles were recovered by centrifugation at 14,000 g for 4 min, and washed twice with deionized water. For PEGylation, the particles were incubated with 2 kDa PEG-SH (Laysan Bio, Arab, AL) in a 3-fold molar excess of PEG-SH to maleimide groups for 1 h at 37 ^{O}C. The resulting particles were centrifuged and washed 3 times with deionized water. The final products were either stored in PBS at 4 ^{O}C.

Synthesis of Gold-nanoparticles decorated ICMVs. 2.2 nm gold core nanoparticles (hydrodynamic size of 5.4 nm) and 4.2nm gold core nanoparticles (hydrodynamic size of 7.4 nm) were incorporated in lipid vesicles, respectively. The incorporation of gold nanoparticles into lipid vesicles was straightforward—Rehydration of dried lipid films with the presence of desired concentration (typical concentration was 0.6 mg/ml) of amphiphilic gold nanoparticles in BTP for the step described in the ICMVs synthesis method, and followed by subsequent steps. A schematic cartoon of synthesis process is illustrated in Figure 3-3.

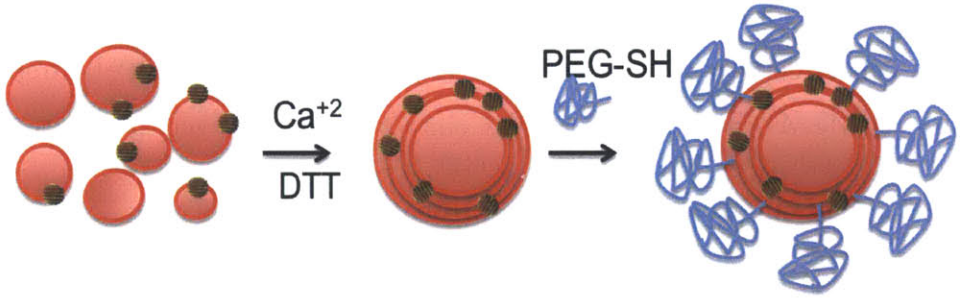

Figure 3-3: Synthesis procedures of gold nanoparticle-decorated lipid vesicle.

Synthesis of Protein encapsulated, and gold-nanoparticles decorated ICMVs. Protein encapsulation was achieved by rehydration of dried lipid films with protein and gold nanoparticles solution in the first step of synthesis described above. The amount of protein used in the studies was 0.3mg/ml of fluorescent OVA (Invitrogen). OVA AF546 or OVA AF488 was used for the studies in this thesis. A schematic cartoon of synthesis process is illustrated in Figure 3-4.

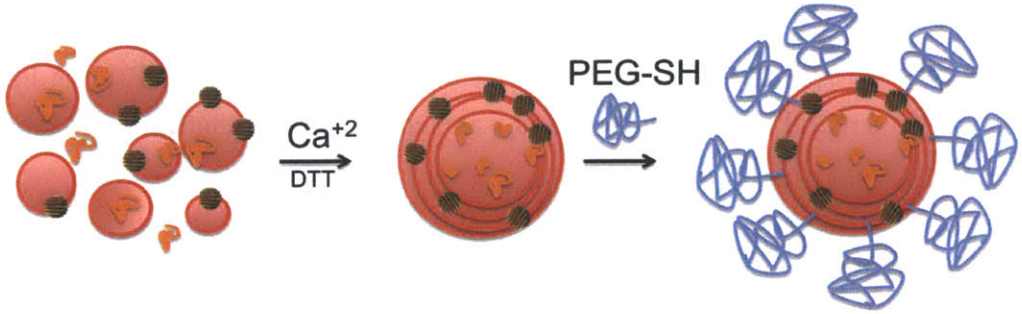

Figure 3-4: Synthesis procedure of protein encapsulated gold nanoparticle-decorated lipid vesicle.

Size Control of Gold Nanoparticle-decorated ICMVs (ICMV-Au). According to dynamic light scattering (DLS) and transmission electron microscopy (TEM), PEGylated ICMV-Au nanoparticles ranges from 50-800 nm (Figure 3-7), with polydispersity index (PI) at 0.34. As-synthesized ICMV-Au was diluted 2 times and passed through a sterile filter twice (200 nm membrane Acrodisc Syringe Filter with HT Tuffryn Membrane, Pall Filters). DLS determined the filtered nanoparticle size was 212 nm with PI= 0.18.

3.2.2 Cell culture

DC2.4 cell line (murine dendritic cells), B16F10 cell line (murine skin melanoma cells), and 4T1 cell line (murine breast cancer cells) were cultured in the studies. 10% FBS, 1% Pen-Strep, 89% complete cell culture medium (DMEM or RPMI) were used. Cells were passaged every 3-4 days.

3.2.3 Protein Encapsulation Quantification

To quantify the protein loading efficiency, fluorescent protein encapsulated ICMVs were treated with 1% Triton X-100 to break down lipid vesicles and the released protein was measured by fluorescent spectrophotometry. OVA quantification assays were also carried out in Hank's buffered saline solution supplemented with 500 ng ml_{-1} of phospholipase A (Sigma, St Louis, MO) [35].

3.2.4 Confocal Laser Scanning Microscopy Imaging

Cells were seeded in an 8-well chamber (Fisher Scientific Lab-Tek™ II Chambered Coverglass) at 60,000 cells per well in 500μL cell culture medium. The cells were allowed to grow overnight to about 80% confluence, and then treated with prepared solutions (typical dosage: 0.6mg/ml gold nanoparticles or 0.1mg/ml lipids) for 3 hours or 18 hours. Cells were washed twice with PBS and subsequently imaged in RPMI (phenol red free) medium. Confocal laser scanning microscopy was performed on a Zeiss LSM 510 using a 63X oil lens, with excitation wavelengths being 488nm, 543nm, and 633 nm.

3.2.5 Transmission Electron Microscopy Imaging of Lipid Vesicles

As-synthesized material in PBS or DI water was diluted x2. 10 uL of solution was places on a formvar coated copper grid, stabilized with evaporated carbon film (EMS, FCF400-Cu). Solution was blotted away using a qualitative filter paper after 20 minutes of deposition. Negative stain, 1% phosphotungstic acid solution (pH=7), was placed on the grid for 10 seconds and blotted away using a qualitative filter paper. The grid was air-dried and stored in TEM grid storage box. TEM imaging was conducted using JEOL 2010 FEG Analytical Electron Microscope at the Center of Materials Science (CMSE) in MIT.

3.3 Results and Discussion

3.3.1 Amphiphilic Gold Nanoparticles loaded on ICMVs

A liposomal amphiphilic gold nanoparticle vector was attempted. This attempted vector was experimentally determined to be inefficacious due to low gold nanoparticle loading efficiency by the presence of visible purple supernatant—free unincorporated gold nanoparticles after centrifugation. Absorbance at 520nm of supernatant was measured by UV-vis.

Because entrapment in unilamellar liposomes was inefficient, we next tested the entrapment of striped gold NPs within multilamellar vesicles (MLVs). Dried lipid layers were rehydrated with an aqueous solution of gold NPs with sonication to create NP-loaded MLVs. TEM imaging in Figure 3-5 shows gold nanoparticles encapsulated in multilamellar liposomes were mostly located in the interior aqueous layers. The darkened regions inside the liposome represent negatively stained hydrophilic water layers.

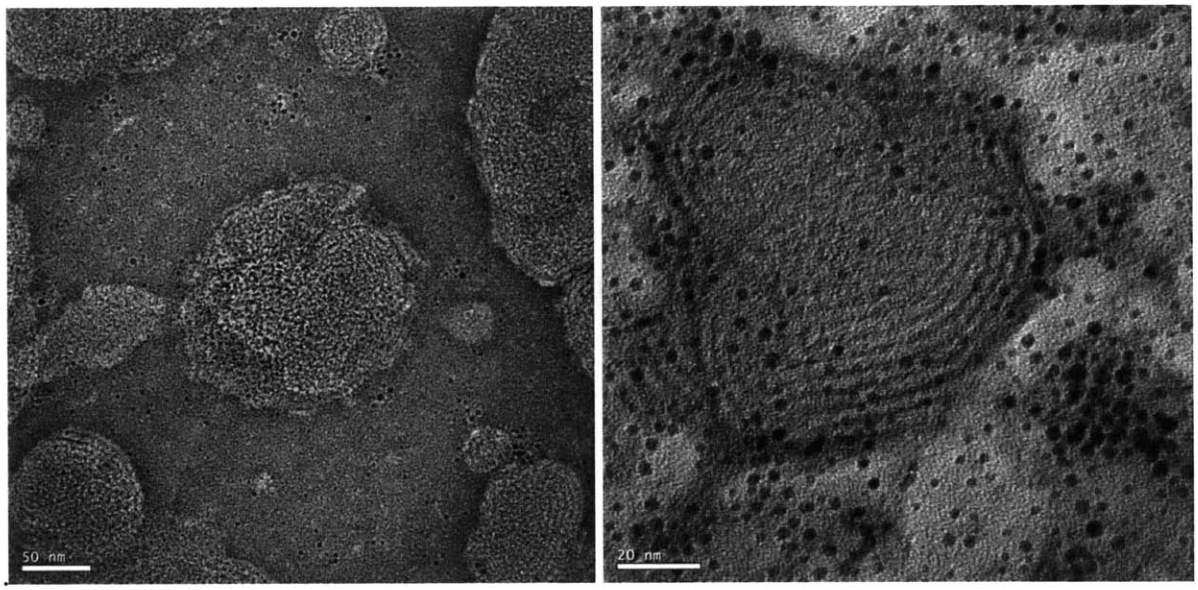

Figure 3-5: TEM image of gold nanoparticle-loaded DOPC liposomes

Next, an ICMV amphiphilic gold nanoparticle vector (ICMV-Au) was attempted. This vector was experimentally determined to be efficacious, exhibiting high gold nanoparticle loading efficiency and high efficiency of centrifugal separation of unencapsulated gold nanoparticles.

Extensive investigation was conducted to optimize ICMV gold nanoparticle loading. Method was described in section 3.2.1. Briefly, lipid films were rehydrated in gold solution to form liposomal Au NPs. Negatively charged unilamellar liposomal gold vesicles were then fused with divalent cations to form multilamellar vesicles. The bilayers were chemically cross-linked to form ICMV-Au. Measurement of absorbance at 520nm via UV-Vis confirmed that the saturation of ICMVs with gold nanoparticles has not yet been observed despite the utilization of gold nanoparticle incubation concentration of 1.2 mg/mL.

Aggregation of gold nanoparticles on lipid vesicles is shown in Figure 3-6. Amphiphilic gold nanoparticle surface energy minimization may be partly responsible for the observed aggregation. Aggregation of this type results in extremes of local gold nanoparticle concentration. Heterogeneous mixtures of this nature are of limited value in clinical applications. Homogenization of ICMV gold nanoparticle loading is the subject of ongoing investigation.

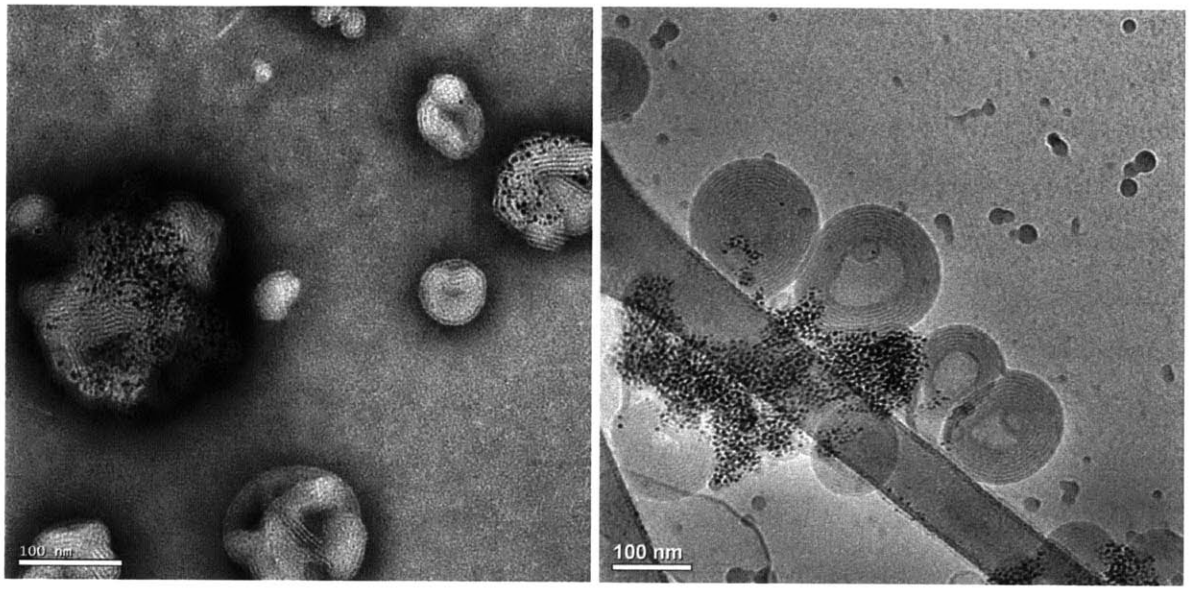

Figure 3-6: TEM image of Gold nanoparticle-loaded ICMVs (left) and Cryo-TEM image of the same sample (right).

The next objective of the design and formation process was size control. Blank ICMV size ranges from 100-700 nm, with 245nm being their mean diameter. This phenomenon was observed via dynamic light scattering (DLS) and TEM as shown in Figure 3-7 (left). ICMV-Au were observed to form in a broader range of sizes, from 50-900 nm. Targeted *in vivo* gold nanoparticle delivery efficiency is inhibited when vesicle size exceeds approximately 200 nm [5].

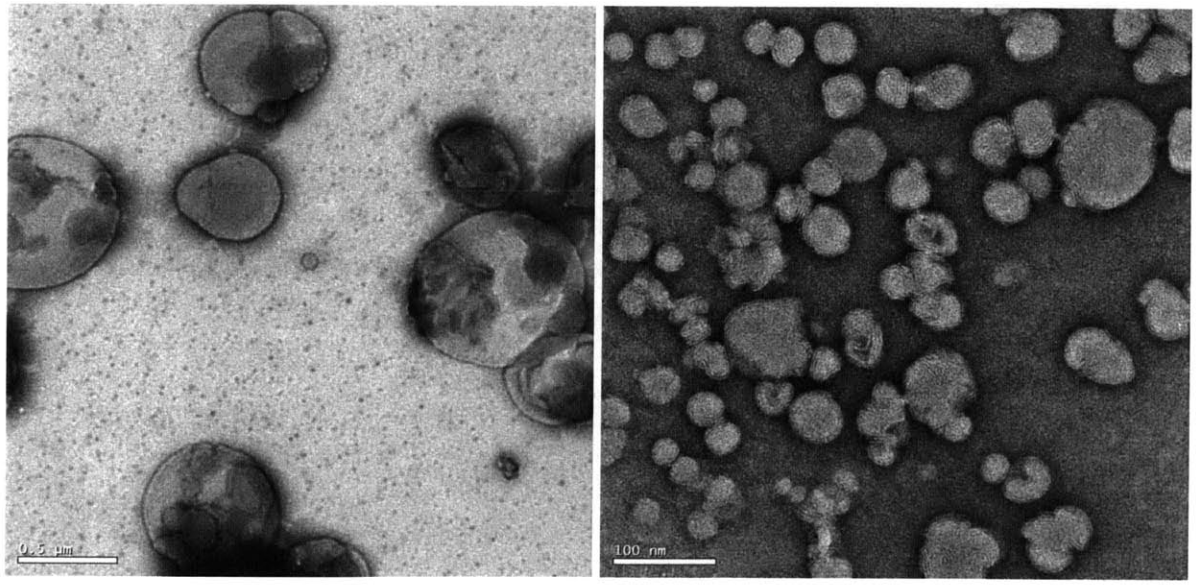

Figure 3-7: TEM images of as-synthesized ICMV (left) and sterile filtered ICMV (right).

Increased sonication of liposomes utilized in ICMV synthesis was an attempted synthesis process modification intended to control ICMV-Au size. This was observed to be ineffective, resulting in as-synthesized ICMV size ranging from 50-900 nm. The distribution of as-synthesized ICMV size was also observed to be unaffected.

Sterile filtration through 200 nm pores was another attempted synthesis process modification intended to control ICMV-Au size. The initial filtration process was observed to be ineffective. ICMVs were almost completely unable to pass through the filter. However, by increasing the degree of PEGylation of ICMVs post-synthesis, these particles were able to pass through a 200 nm pore filter. The size range observed in post-filtration ICMVs was 50-200 nm. Figure 3-8 shows excess PEGylated filtered ICMV-Au. Figure 3-9 shows cryo-TEM images of excess PEGylated filtered blank ICMV and ICMV-Au. Structural deformation was not observed in post-filtration ICMVs of either type.

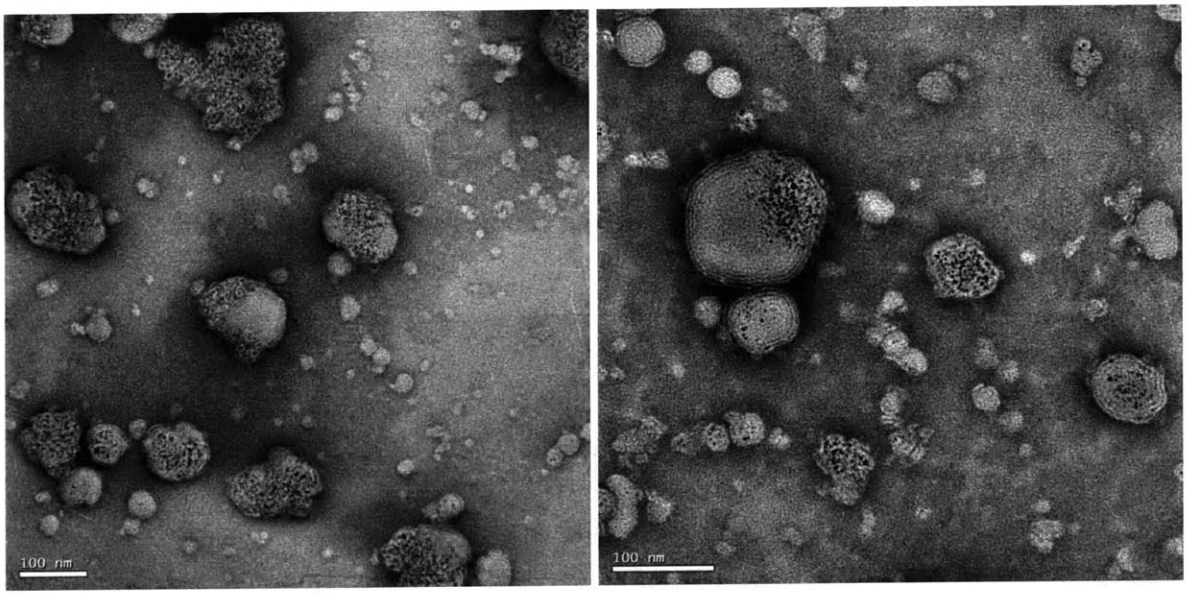

3-8: Sterile filtered ICMV-Au

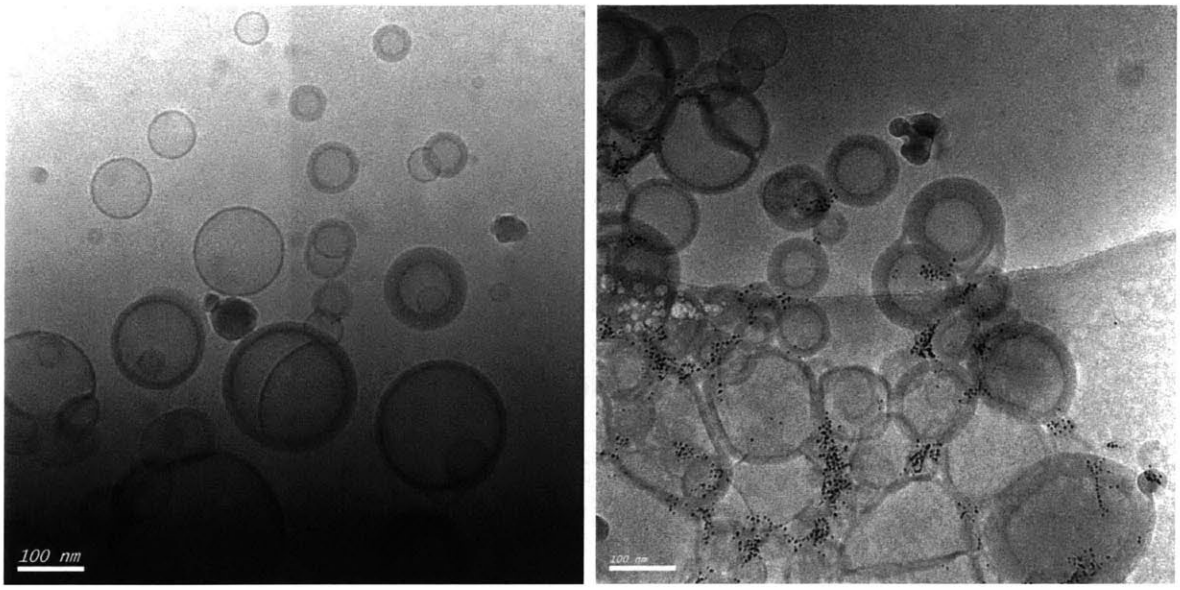

3-9: Cryo-TEM images of sterile filtered ICMVs (left) and Sterile filtered ICMV-Au (right).

Gold nanoparticles in the above experiments were all of the same dimensions. The gold nanoparticle core and hydrodynamic diameters were 2.2 nm and 5.4 nm, respectively. Bilayer thicknesses in the above experiments were approximately 5 nm. Similarity between gold nanoparticle hydrodynamic size and bilayer thickness correlates to high nanoparticle solubility in lipid bilayers.

Having established the procedure for efficient gold nanoparticle incorporation into ICMVs, the above incorporation experiments were repeated using gold nanoparticles of larger diameter. The large gold nanoparticle core and hydrodynamic diameters were 4.2 nm and 7.4 nm, respectively.

ICMV-synthesis membrane fusion and cross-linking were observed to be inhibited by the presence of gold nanoparticles whose hydrodynamic diameter exceeded the bilayer thickness. Resultant vesicles were liposomal and contained linear aggregated gold nanoparticle not observed in liposome or ICMV synthesis experiments using the previous gold nanoparticle size (2.2/5.4 nm). The interesting linear aggregation is speculated to result from the balance between minimization of bilayer deformation and electrostatic interaction of nanoparticles.

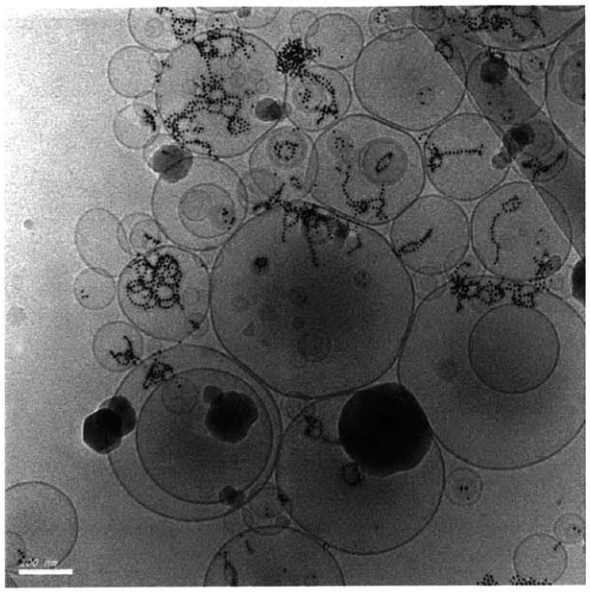

Figure 3-10: Cyro-TEM image of 4.2nm gold nanoparticles incorporated in lipid vesicles.

3.3.2 Cellular Uptake of Gold Nanoparticle-Decorated Lipid Vesicles

The radiotherapeutic efficiency of ICMV-Au is postulated to be dependent on the intracellular Au spatial distribution. Cellular internalization pathways of nanoparticles are shown in Figure 3-11. Striped gold nanoparticles has been observed to enter cells through both endocytic and non-endocytic pathways. However, the intracellular spatial distribution of ICMV-Au remained unknown, which was experimental determined in the following work.

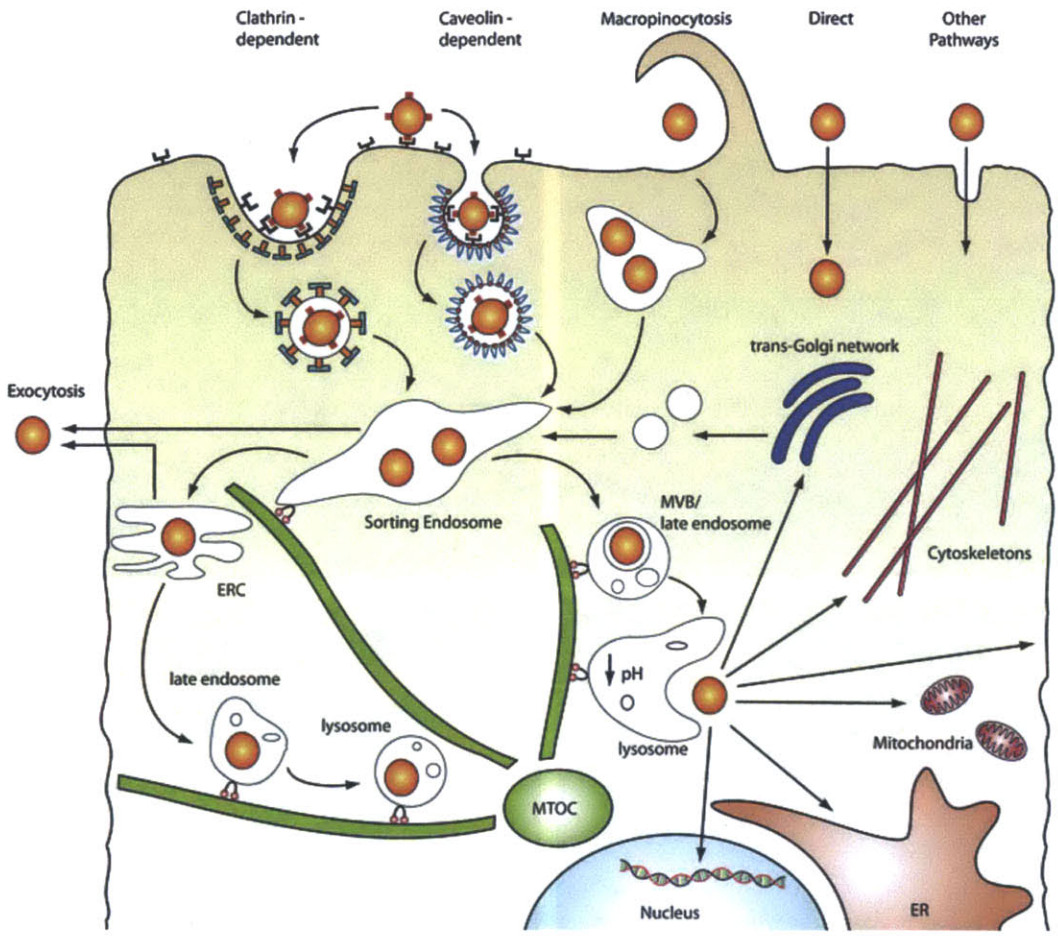

Figure 3-11: Intracellular internalization pathways of nanoparticles. Illustration adapted from reference [13]

Lipids used in ICMV synthesis contained 1% NBD-DOPC. Gold nanoparticles were dyed with BODIPY. ICMV synthesis was altered to encapsulate OVA-AF546. These steps were taken to facilitate determination of intracellular ICMV-Au spatial distributions. These ICMVs were then incubated *in vitro* with target cells. Confocal microscopy was used to image the intracellular spatial distributions of the markers described above.

Dendritic cells were incubated with unfiltered ICMV-Au without excess PEGylation. Figure 3-12 shows that unfiltered ICMV-Au was too large to undergo endocytosis within a 3 hour incubation. Intercellular nanotube formation was observed. This phenomenon is unexplained as of the writing of this thesis.

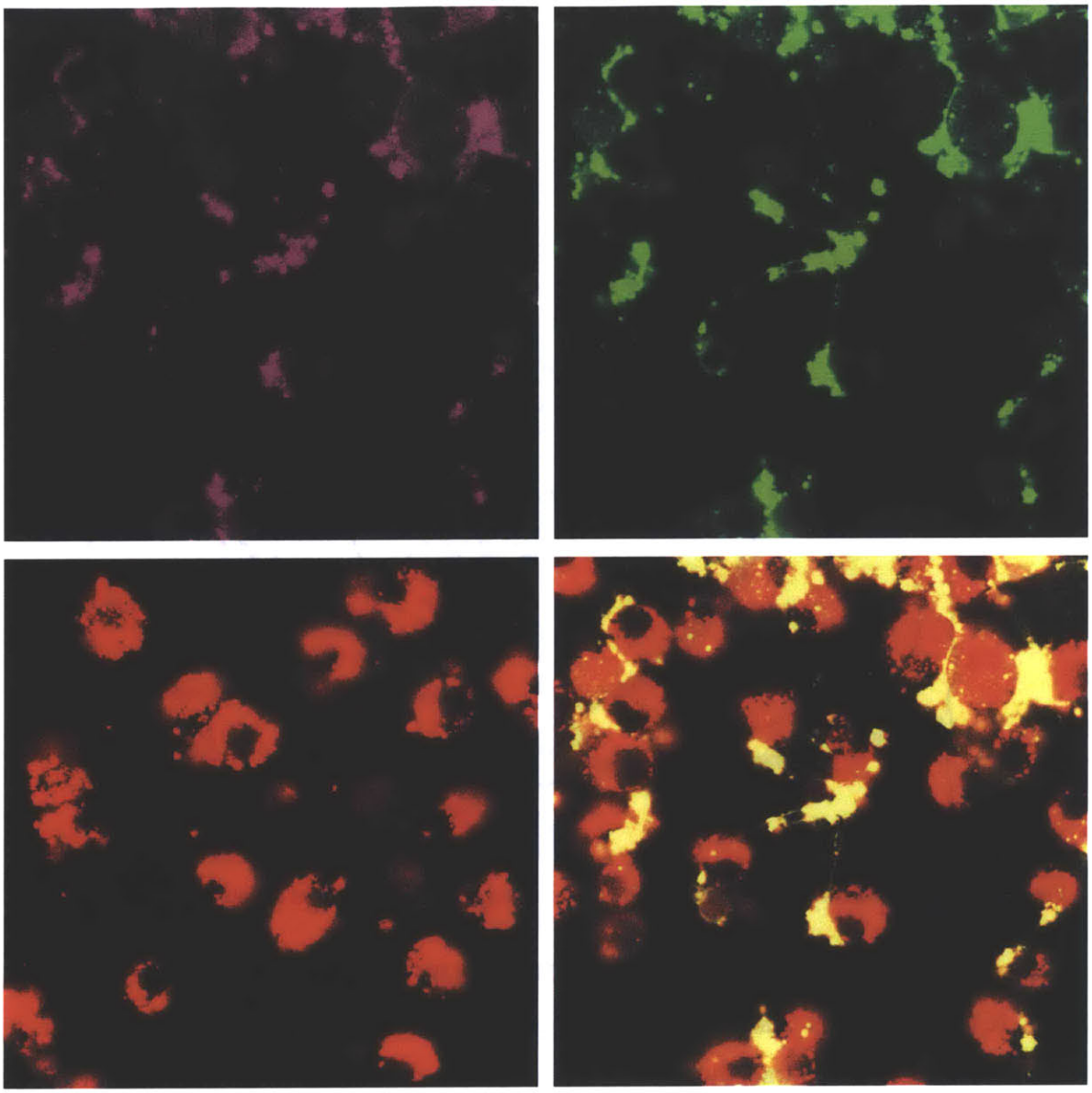

Figure 3-12: ICMV(green)-Au (pink)-OVA(red) treated mouse dendritic cells. Some ICMV-Au-OVA nanoparticles were internalized, while others (potentially larger nanoparticles) were stuck on the outermost membrane of the cells.

Soluble Au was incubated with B16F10 and 4T1 cells. Figure 3-13 shows that soluble Au equilibrated to a uniform intracellular spatial distribution in B16F10. In 4T1, soluble Au underwent endocytosis, and a significant proportion of Au was confined to endolysosomes. Confocal microscopic resolution limited the precision of intracellular spatial distribution determination. Future work will utilize thin-section TEM to more precisely determine the intracellular Au spatial distribution.

Figure 3-13: Soluble gold nanoparticle-treated B16F10 (left) and 4T1 cells.

Filtered and unfiltered excess PEGylated ICMV-Au were incubated with 4T1 cells for 3 and 18 hours. Limited cell entry by unfiltered ICMV-Au was observed within a 3 hour incubation, whereas a significant amount of cell entry by filtered ICMV-Au was observed in the same time interval. Significant amounts of cell entry by both filtered and unfiltered ICMV-Au was observed after 18 hour incubations. Figure 3-14 shows images of the above mentioned situations.

Filtered and unfiltered ICMV-Au were confined in endolysosomes after 18 hour incubations. ICMVs that entered 4T1 cells were not degraded and their gold nanoparticles were not able to migrate freely in cytosols. This observation is counter to the general trend that gold nanoparticles tend to be able to migrate from one membrane to another.

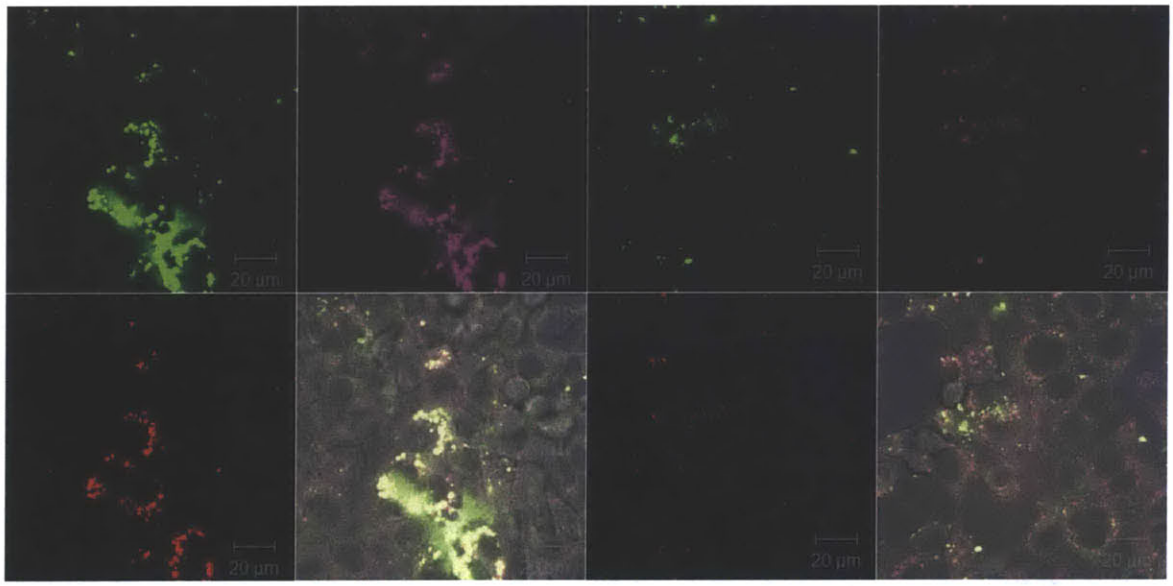

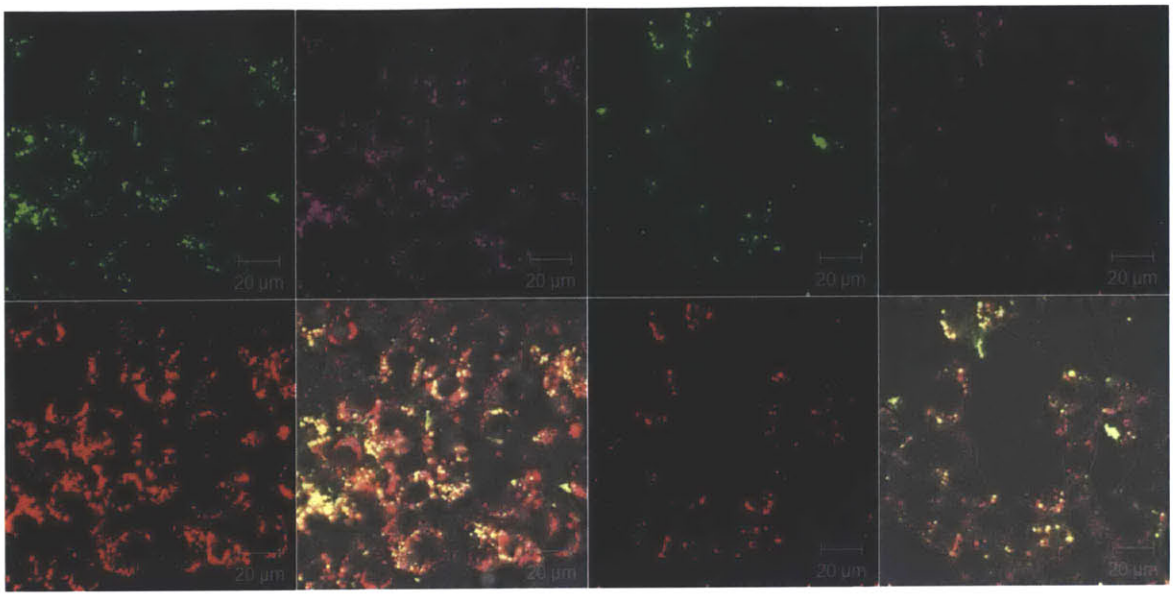

Figure 3-14 : ICMV(green)-Au (pink)-OVA(red) treated 4T1 mouse breast cancer cells. 4T1 cells after 3 hours of incubation with ICMV-Au-OVA (upper left) and 18 hours of incubation (lower left) at 37 °C; 4T1 cells after 3 hours of incubation with "sterile filtered" ICMV-Au-OVA (upper right) and 18 hours of incubation (lower right) at 37 °C.

Figure 3-15 shows results for the above procedure repeated using B16F10 target cells. Cell entry by filtered and unfiltered ICMV-Au was observed after 3 hour incubations. Intracellular gold nanoparticle migration from both filtered and unfiltered ICMV-Au was observed after 18 hour incubations. Intracellular diffusion of NBD-DOPC was observed. This observation implies either ICMV degradation or NBD-DOPC migration.

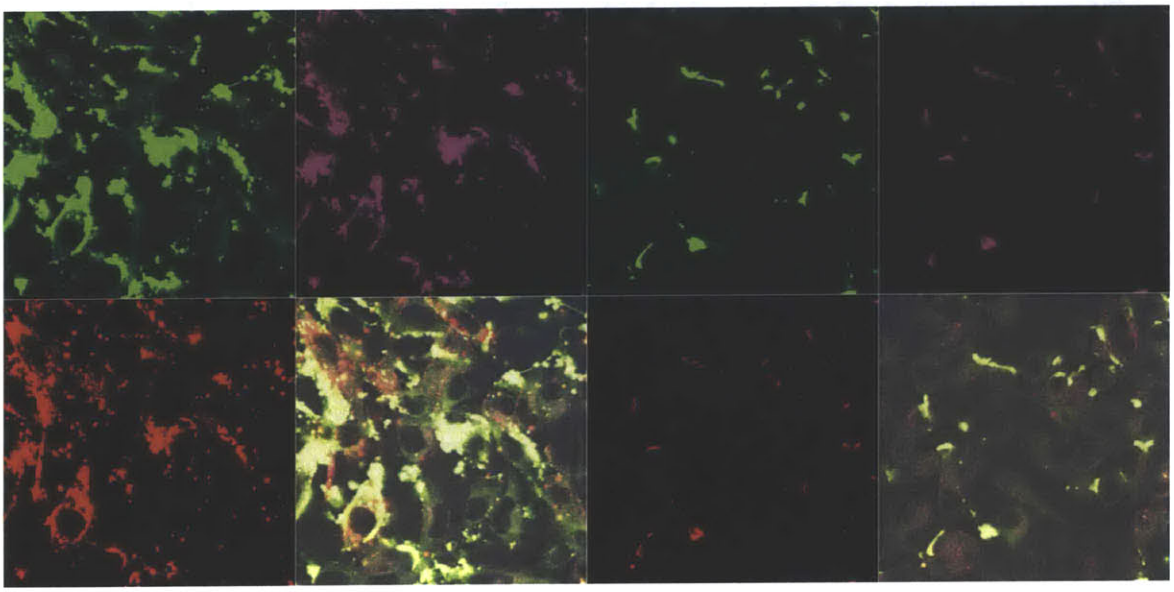

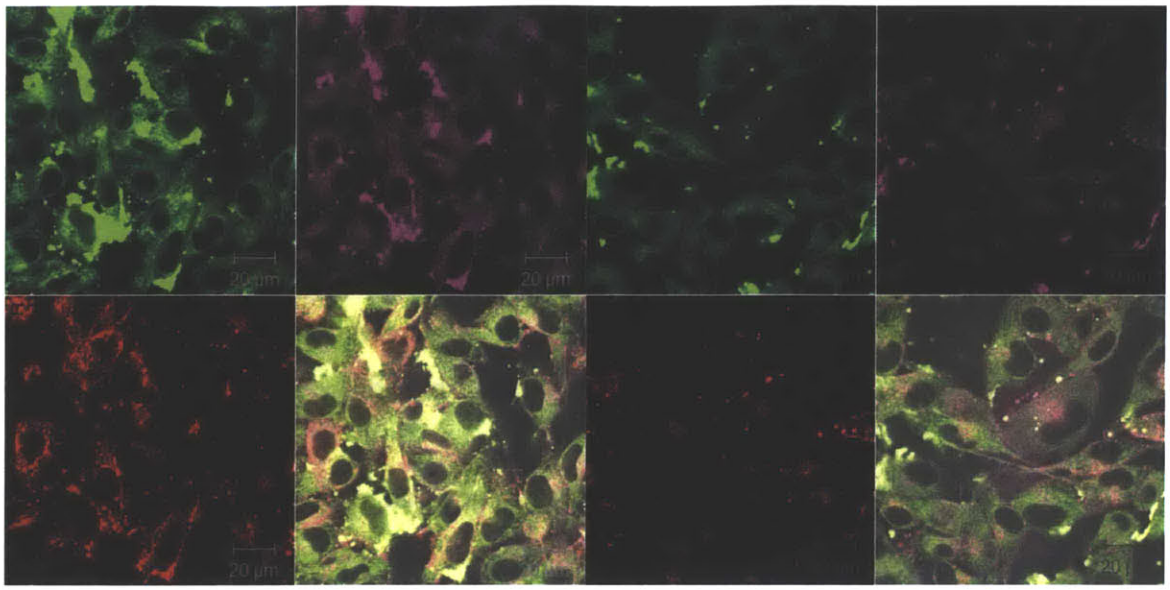

Figure 3-15 : ICMV(green)-Au (pink)-OVA(red) treated B16F10 mouse melanoma cancer cells. B16F10 cells after 3 hours of incubation with ICMV-Au-OVA (upper left) and 18 hours of incubation (lower left) at 37 °C; B16F10 cells after 3 hours of incubation with "sterile filtered" ICMV-Au-OVA (upper right) and 18 hours of incubation (lower right) 37 °C.

3.4 Conclusion

Experimental methods were developed for ICMV synthesis, gold nanoparticle loading efficacy qualification, ICMV-Au size control, gold nanoparticle size sensitivity qualification, and delivery spatial distribution qualification.

Sterile filtration of ICMV-Au through 200 nm pores was able to produce a prospective clinical treatment vector. ICMVs loaded with 2.2/5.4nm Au were not observed to reach saturation even at 1.2mg/mL, while 4.2/7.4nm Au saturated at 0.6mg/mL. Further increase of loading efficiency will be investigated in future work by saturating ICMVs with 2.2/5.4nm Au.

Post-delivery spatial distribution of this vector was examined for two cell lines at two time points. These distributions were observed to be sensitive to the target cell type. The efficacy of this vector as a radiosensitizer is quantified in Chapter 5.

4 Interaction of Amphiphilic Gold Nanoparticles with Lipid Membrane

4.1 Introduction

Striped gold nanoparticles enter cells through both endocytic and energy-independent non-endocytic pathways [45]. However, the mechanism of cell membrane penetration is not very well understood. Here, we aimed to study the membrane penetration mechanisms with synthetic membranes that mimic natural cell membranes.

We also investigated the correlation of lipid composition with gold nanoparticles' membrane migration ability. The ultimate goal is to find a composition that amphiphilic gold nanoparticles could not pass through once they were trapped in the lipid bilayers. If nanoparticles loaded in vesicles were able to pass through membranes, the efficacy of gold nanoparticles targeted delivery *in vivo* would be very low due to the loss of nanoparticles transferred to adjacent membranes in blood vessels before reaching targeted sites where various membranes are present.

4.2 Experimental Methods

4.2.1 Synthesis of Giant Multilamellar Vesicles

Giant multilamellar vesicles (GMVs) were synthesized as model membranes in order to study how membrane composition, curvature, and fluidity affect the penetration ability of striped gold nanoparticles. The synthesis process is as follows: 6 mmoles of desired lipids in chloroform were dried under nitrogen flow, and the residual chloroform was evaporated in a chemical hood overnight. Dried lipids in glass vials were kept cap off and hydrate in a 70°C water bath for 2-6 hours. 2 mL of 50 mM sucrose in PBS or water was then added to rehydrate the lipids in a 70°C water bath for formation of GMVs overnight. GMVs were harvested and stored at 4 °C.

4.2.2 Synthesis of Gold and Protein Co-loaded Liposomes

DOPC liposomes loaded with fluorescent OVA AF 546 and gold nanoparticles (2.2 nm) were synthesized by rehydration of dried lipid films with gold/ OVA mixed solution. 15 mM dried DOPC lipids were rehydrated with 0.15 mg/mL gold nanoparticles and 0.3 mg/mL OVA in PBS. The solution was vortexed for 30 seconds every 10 minutes for an hour, followed by six freeze and thaw cycles (1 minute in liquid N_2 and 3 minutes in 37°C water bath). Extrusion through a 200 nm membrane was conducted 21 times. Excess gold and OVA were removed by either centrifugation using Airfuge at the highest speed for 30 minutes 2 times or 300kDa dialysis cassette. Final particle size was confirmed by DLS.

4.2.3 Confocal Laser Scanning Microscopy Imaging

30 uL of GMVs was added to each single well in the lab-tek chamber. 30 uL of gold nanoparticles in PBS was added to the chamber, and 50 mM glucose in PBS was then topped the chamber to 200 uL volume. Incubation was conducted for three hours at 25 ° C.

4.3 Results and Discussion

4.3.1 Visualizing Membrane Penetration Capability of Striped Gold Nanoparticles

Striped gold particles (gold core diameter 2.2nm) labeled with bodipy 650/665 dye were incubated with GMVs (DOPC 80% DOPG 20%) for 3 hours at 25 ° C in PBS. GMVs were composed of 20% DOPG to achieve an overall negatively charged surface to mimic cell membrane. Confocal microscopic imaging showed effective gold nanoparticle penetration into the GMVs and localization in the membrane bilayers (Figure 4-1).

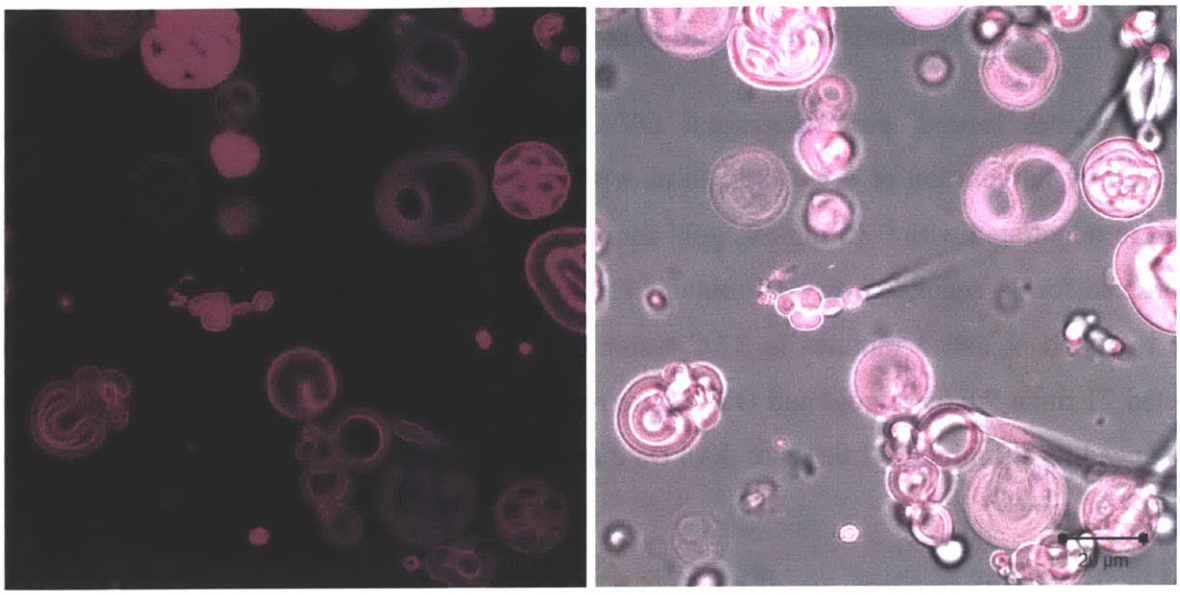

Figure 4-1: Bodipy channel (left) and bright field overlay (right) showed GMV membranes are labeled with striped gold nanoparticles.

To determine if the GMVs were intact, soluble fluorescent protein OVA-AF546 was added to the GMV/gold nanoparticle solution and incubated with them for three hours at 25 ^{o}C. The proteins were all excluded outside of GMVs, indicating that GMVs were intact and gold nanoparticles can penetrate from the outer membrane to inner membranes without disruption of membrane integrity (Figure 4-2).

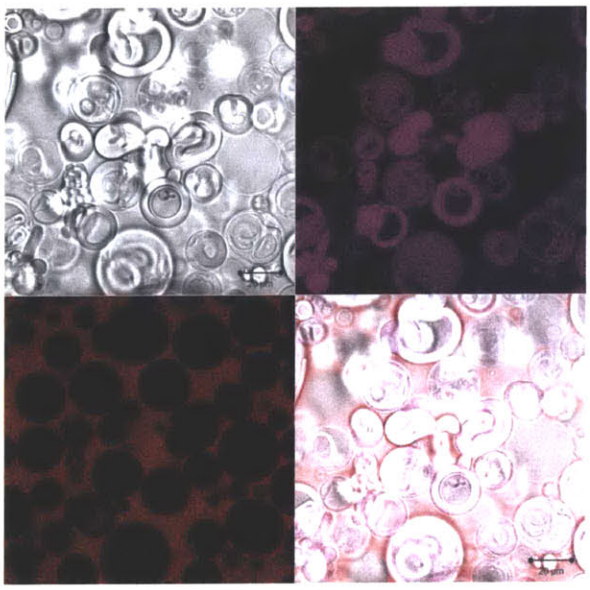

Figure 4-2: Upper left: bright field; upper right: gold nanoparticles (pink); lower left: OVA 546 (red); lower right: overlay of three channels. Scale bar = 20um.

The next objective was to determine how polyethylene glycol (PEG) affects the penetration ability of gold nanoparticles. PEG is a well-known polymer that is highly biocompatible and hydrophilic which provides steric hindrance against non-specific protein adsorption to surfaces of nanoparticles [8]. However, our experiments indicated that GMVs containing up to 20 mol% of PEG-DOPE not hinder the penetration ability of gold nanoparticles into the vesicle membranes (Figure 4-3). Notice that addition of lipid-PEG molecules generated smaller and uniformly-shaped GMVs because PEG is also known as to stabilize membrane curvature [4].

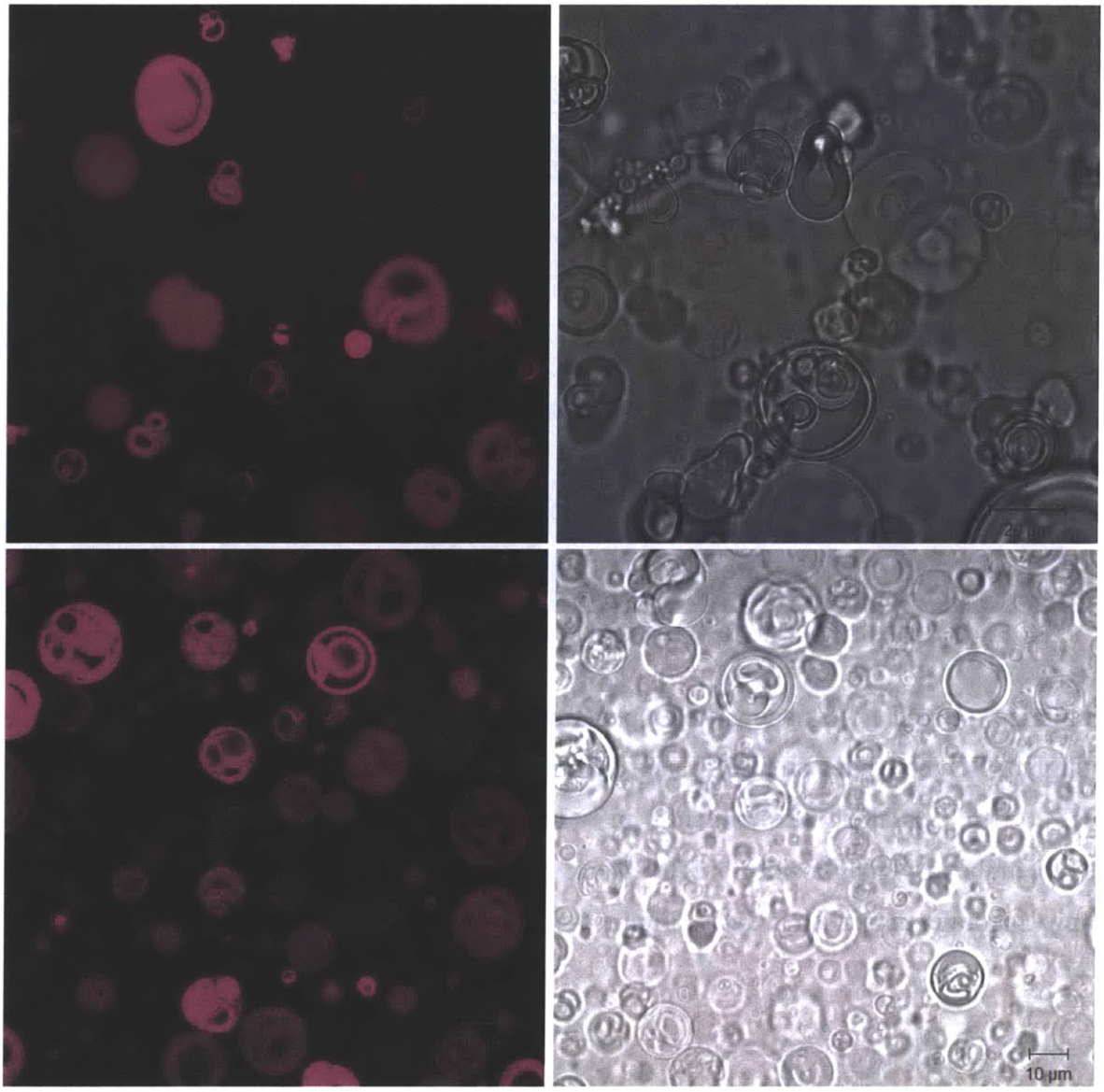

Figure 4-3: Gold nanoparticles labeled DOPC (80%) DOPG (20%) GMVs (upper panel); Gold nanoparticles labeled DOPC (80%) DOPE-PEG 2K(20%) GMVs (lower panel).

Membrane fluidity is another important factor affecting gold nanoparticles penetration ability. Membrane fluidity can be lowered by the addition of lipids with higher gel-liquid crystal transition temperature (T_m). Unsaturated fatty acids and shorter hydrocarbon chain in lipid tails lower the T_m of a polymer chain. To evaluate whether a more packed membrane will influence the penetration ability of striped gold nanoparticles, we decreased the membrane fluidity of GMVs by addition of 20% DOPS-PEG 2000 in matrix DOPC. Increasing membrane rigidity did not affect the penetration of gold nanoparticles to membrane (Figure 4-4).

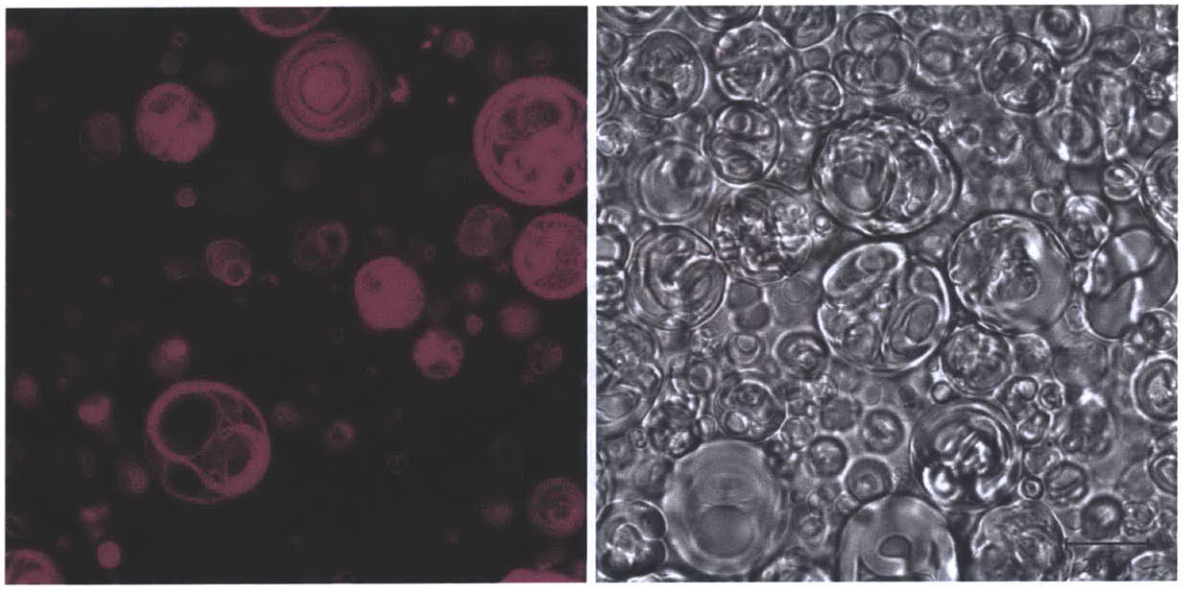

Figure 4-4: DOPS-PEG 2000 (20%) DOPC (80%) vesicles incubated with striped gold nanoparticles.

To summarize, striped gold nanoparticles penetrate synthetic membrane effectively within an hour. Interestingly, PEG molecules on membranes did not block the membrane penetration capability of these particles. In parallel experiment in our laboratory, we have found that GM1 (monosialotetrahexosylganglioside) might block penetration of gold nanoparticles to membranes (Prabhani Atukorale, unpublished data). Figure 4-5 shows the composition of PEG and GM1.

a)

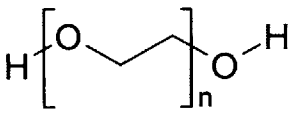

b)

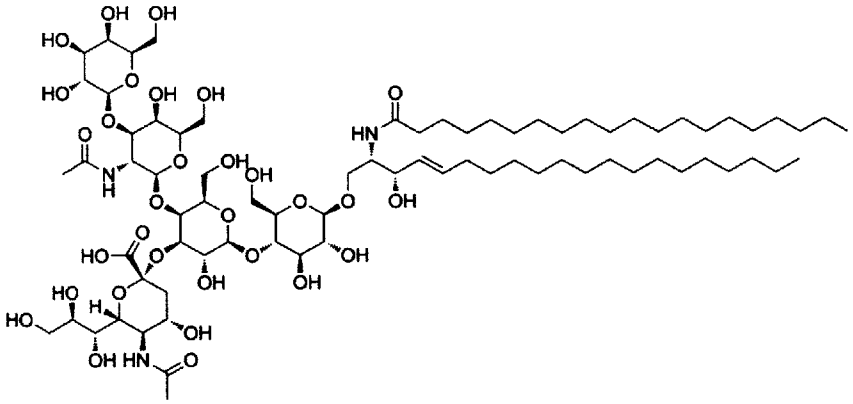

Figure 4-5: a). PEG molecule and b). GM1 chemical structure

4.3.2 Membrane Hopping Ability of Gold Nanoparticles from Liposomes or ICMVs to GMVs

The next objective was to determine if the particles will migrate from one membrane to another. If so, will migration of gold nanoparticles loaded on liposome membranes result in fusion of liposome membranes and GMV membranes? To answer these questions, we loaded membrane interactive striped gold nanoparticles into liposome membranes while simultaneously encapsulating fluorescent OVA proteins. Free unencapsulated fluorescent OVA proteins were then removed by dialysis. We hypothesize that if gold nanoparticles promote membrane fusion, the encapsulated OVA will be transferred from liposomes to GMVs during the fusion process. If not, we will only see signals from gold nanoparticles on GMV membranes but not OVA signals (See Figure 4-6 for schematic view).

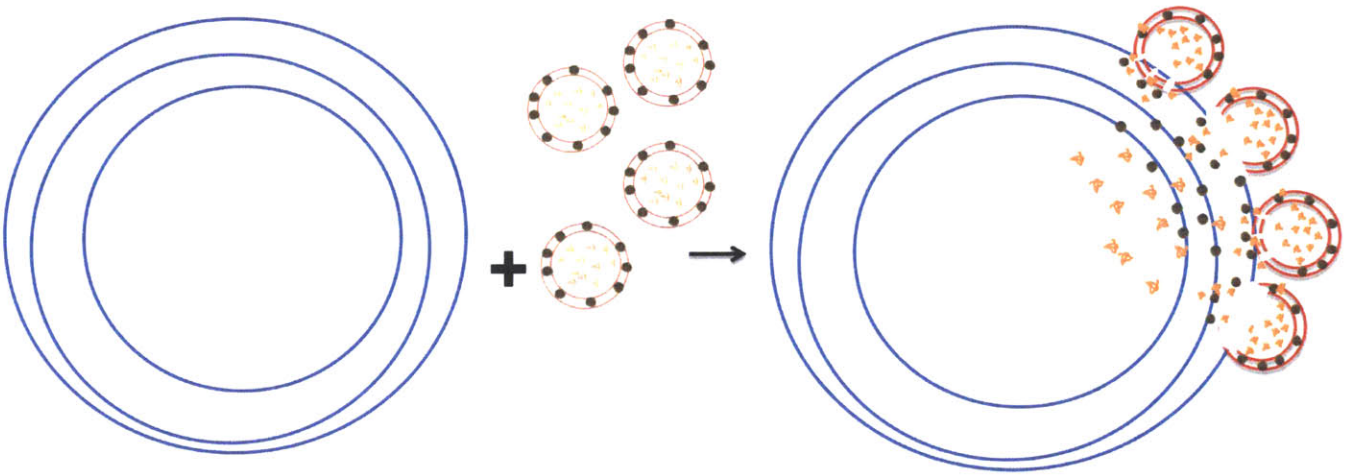

Figure 4-6: Membrane fusion promoted by membrane interactive amphiphilic gold nanoparticles migrating from liposomes (red) to GMVs (blue). Fluorescent proteins (OVA AF546) were encapsulated in liposomes to track the integrity of liposomal membrane after particles transferring. Hypothesis 1: gold nanoparticles promoted membrane fusion during migration from liposomal membrane to GMV membrane.

To generate liposomes with embedded striped NPs, PBS that contained OVA AF546 and striped gold nanoparticles (MUSOT 1:1) was added to rehydrate dried DOPC lipid films to form vesicles. In order to compare the membrane migration ability, liposomes formed with the presence of protein but lacking gold nanoparticles were also prepared. These liposomes with proteins encapsulated were then incubated with striped gold nanoparticles for an hour before addition to the GMVs solution.

We then incubated Au NP-loaded liposomes with GMVs (DOPC or DOPC/DOPG 4/1) to examine the interaction of gold-loaded liposomes with the larger multilamellar vesicles, as a model for the interaction of Au-loaded liposomes with cell membranes. Gold nanoparticle-decorated liposomes added to GMVs in PBS adsorbed on GMV membranes, and gold nanoparticles were observed to migrate from liposomal membrane to the inner membranes of GMVs. We characterized this process as "hopping" or "migration" because there was no protein signal observed in GMVs, which implied that gold nanoparticles transferred from membrane to membrane without generation of stable pores (Figure 4-7 and 4-8). Notice that the membrane adsorption phenomenon only appeared in pure DOPC liposomes and DOPC GMVs. Gold nanoparticle-loaded DOPC liposomes did not adsorb to DOPC/DOPG GMVs at all, however, gold nanoparticles were still able to migrate to GMV membranes (Figure 4-9)

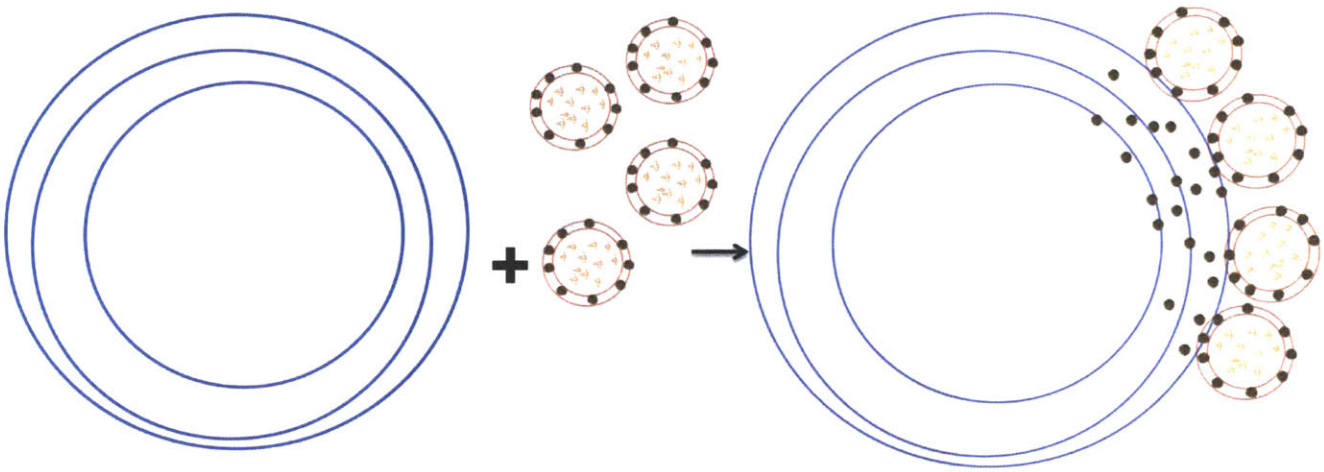

Figure 4-7: Membrane fusion promoted by membrane interactive amphiphilic gold nanoparticles migrating from liposomes (red) to GMVs (blue). Fluorescent proteins (OVA AF546) were encapsulated in liposomes to track the integrity of liposomal membrane after particles transferring. Hypothesis 2: gold nanoparticles did not promote membrane fusion during migration from liposomal membrane to GMV membrane.

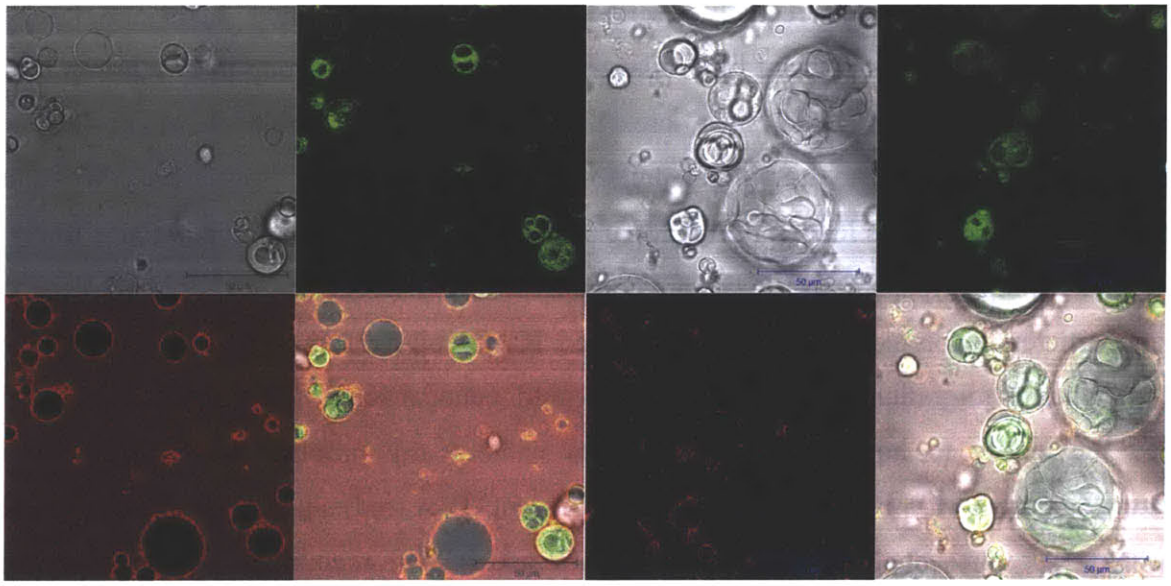

Figure 4-8: Liposomes formed in the presence of gold nanoparticles (left) adsorbed to DOPC GMVs membranes and striped gold nanoparticles (green) were able to penetrate through GMV membranes without membrane disruption. Proteins (red) encapsulated inside liposomes were colocalized on GMVs membranes but not inside GMVs as predicted in Fig. 5-7. In contrast, protein-encapsulated liposomes "post-loaded" with gold nanoparticles adsorb less efficiently on GMV membranes. However, gold nanoparticles were still able to distribute on liposome and GMV membranes evenly.

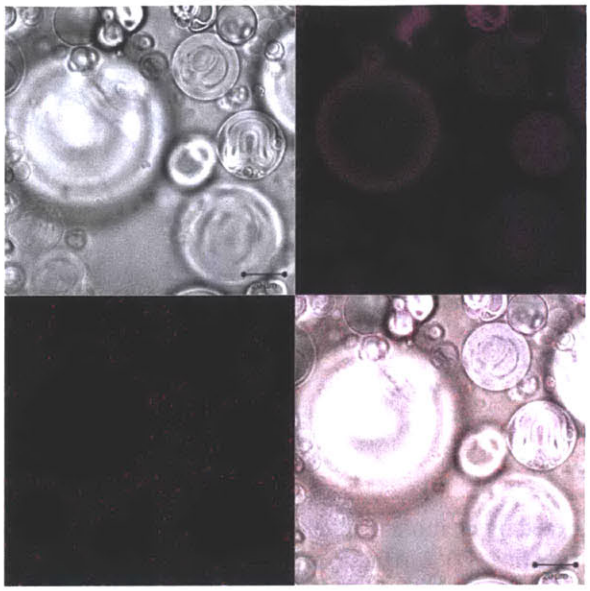

Figure 4-9: DOPC/ DOPG 80/20 GMVs incubated with gold and OVA-546 loaded DOPC Liposomes.

Gold nanoparticles loaded into MLVs or liposomes can hop freely between adjacent membranes within an hour. However, our laboratory recently described a novel class of "stapled" liposomes, lipid capsules whose walls are composed of stacked lipid bilayers connected by headgroup-to-headgroup interbilayer covalent crosslinks [35]. These interbilayer –crosslinked multilamellar vesicles (ICMVs) show enhanced stability in serum compared to traditional unilamellar or multilamellar liposomes. We thus tested whether striped gold particles loaded into ICMVs would still "hop" to GMV membranes freely as seen with Au-loaded simple liposomes. ICMVs are composed of very closely stapled lipid bilayers; therefore, gold nanoparticles decorated in the densely packed ICMV bilayers may be highly stable and have limited membrane migration ability. Strikingly, gold nanoparticles incorporated into ICMVs still presented the ability to hop between membranes without any problem within an hour at room temperature (Figure 4-10). ICMVs (green) and fluorescent OVA (red) signals colocalized, whereas gold nanoparticles were presented uniformly in both GMV and ICMVs membrane, which showed that they hopped from ICMVs to GMVs and spread evenly in all of the lipid membranes in PBS.

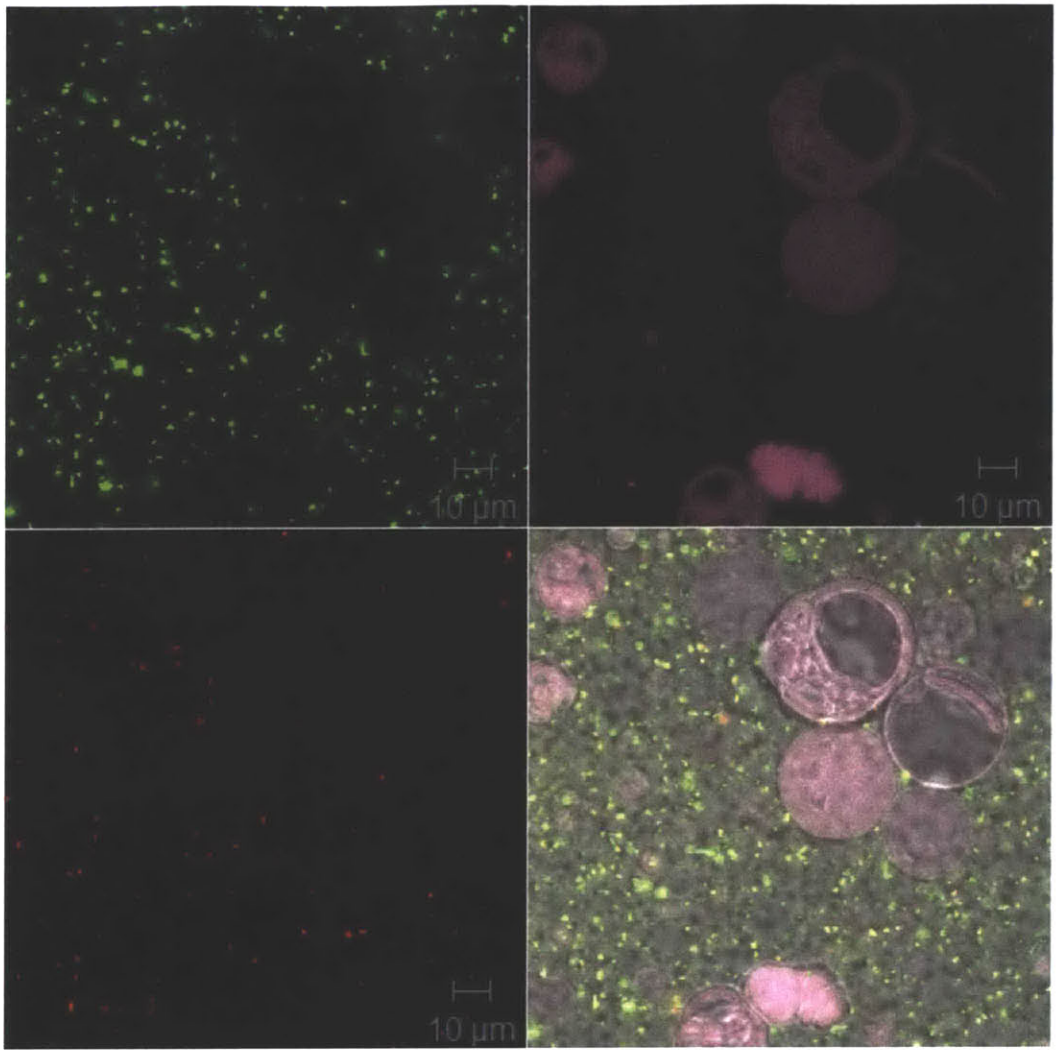

Figure 4-10: Fluorescent OVA 546 encapsulated (red) gold (pink) decorated-ICMVs (green) incubated with DOPC (80%) DOPG (20%) GMVs in PBS. Gold nanoparticles in ICMV bilayers can hop freely from their original bilayer in ICMVs to GMV membranes.

4.4 Conclusion

MUS:OT 1:1 striped gold nanoparticles were known to have the capability to penetrate cell membranes through non-endocytic pathways. Using synthetic lipid membrane vesicles to model cell membranes sans surface proteins, we have studied the interaction of MUS:OT 1:1 striped gold nanoparticles with lipid bilayer membranes. We have investigated the interaction of striped gold nanoparticles with lipid membranes of manifold compositions and curvatures.

In all cases, striped gold nanoparticles were capable of penetrating and residing in lipid bilayers without rupturing the membranes. Freely solubilized OVA was not observed in lipid vesicle aqueous

cores while gold nanoparticles were observed in both inner and outer lipid membranes. Striped gold nanoparticles were also observed to migrate from liposomes, MLVs, and ICMVs onto GMV membranes without causing membrane rupture.

According to these observations, synthetic lipid membranes with embedded striped gold nanoparticles may prove a highly efficacious vector for the delivery of gold nanoparticles to cell membranes *in vivo*. Endocytosis of ICMVs containing embedded striped gold nanoparticles may result in migration of striped gold nanoparticles from ICMVs in cytosols or endolysosomes to the cell's outermost lipid membrane. X-ray irradiation of the striped gold nanoparticle decorated cells may then rupture the cells' membranes. Energy deposition from incident X-rays is concentrated on the gold nanoparticles due to gold's high atomic number, producing energetic free electrons which dissociate lipid molecules in the immediate vicinity of the gold nanoparticles. It is therefore envisioned that selective migration of gold nanoparticles onto oncogenic cells and subsequent X-ray irradiation could form the basis of a clinical treatment of carcinoma.

5 Gold Nanoparticles as Radiosensitizers for Cancer Therapy *in vitro*

5.1 Background

Since 1895, radiotherapy has been a subject of intense interest. It managed to capture the public's imagination early on, despite many early disastrous results. Ironically, radiotherapy is now used to *cure* some types of cancer.

More recently, radiotherapy has been amongst physicians' primary clinical cancer treatments and been observed to be efficacious, particularly in conjunction with chemotherapy. Unlike near infrared electromagnetic radiation, x-ray or gamma-ray radiation can penetrate on the order of inches or feet into living tissue and are used to treat deeply seated tumors. Nearly two-thirds of all cancer patients will receive radiation therapy during their illness. Urgent needs in clinical for improvement of radiotherapy has remarkably motivated the development of radiosensitizers and radioprotectors [21]. Improvements include the use of megavolts X-ray to avoid skin damage, tomotherapy and intensity-modulated radiation therapy (IMRT) to better concentrate the dose within the shape of the lesion. Despite these advances, radiotherapy fails to eradicate tumors due to the limited dosage applied to reduce damage of the surrounding tissues. To date there has been no eloquent means by which to bypass this trade off between beam intensity, cumulative dose, lesion damage, and healthy tissue damage, particularly to sensitive organs or regions such as the brain, ovaries, and neck.

In addition to dose reduction to minimize side effects, radiosensitizers such as inorganic nanoparticles are used to enhance the effect of radiotherapy [28]. Gold nanoparticles, as a high Z material, can generate auger electrons and photoelectrons that amplify the photon-matter interactions and enhance therapeutic efficacy of x-ray and gamma ray irradiation. Ionization of cellular compartments or water molecules can induce cell death by membrane rupture, radiolysis, and DNA damage [22]. Apoptosis resulting from lipid peroxidation can be induced by hydroxyl radical [30][34].

Incident photon energy significantly affects the radiosensitization efficacy of gold nanoparticles (Figure 5-1). Besides gold, iodine is another commonly used radiosensitizer, however, gold is hypothesized to exhibit superior radiosensitization efficacy between 80 keV and 800 keV (Figure 5-1) [21].

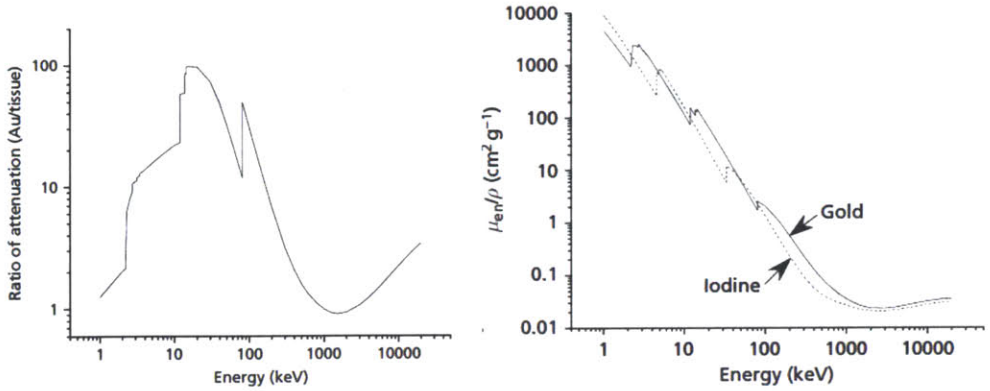

Figure 5-1: Ratio of gold attenuation compared with soft tissue for the same thickness (gcm^{-1}) of the two materials. A factor of ~1—is obtained at ~20 keV. (left); Local energy absorption coefficients of gold and iodine versus X-ray energy. Plots adapted from [21].

Membrane interactive striped gold nanoparticles equilibrate to a homogeneous spatial distribution in some cell types such as B16F10 and DC2.4. The resulting homogenization of x-ray dose applied to striped gold nanoparticle loaded target cells may enhance radiolytic killing efficiency (Figure 5-2).

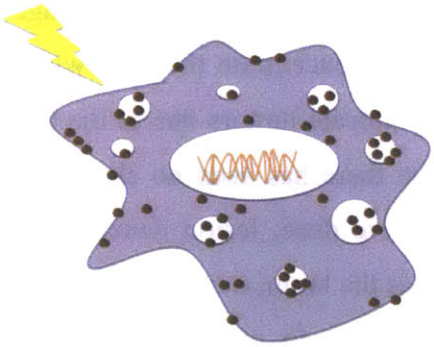

Figure 5-2: Concept of Au NPs as radiosensitizers for enhanced radiotherapy

A schematic cartoon in Figure 5-3 illustrate the concept of membrane damage induced by energetic electrons via the interaction of ionizing radiation with gold nanoparticles, triggering leakage of molecules from the bilayer vesicles. One potential application is the development of ionizing radiation triggered drug release. This work has evaluated striped gold nanoparticle enhanced radiolysis in general, with particular focus on cell membrane rupture induced necrosis.

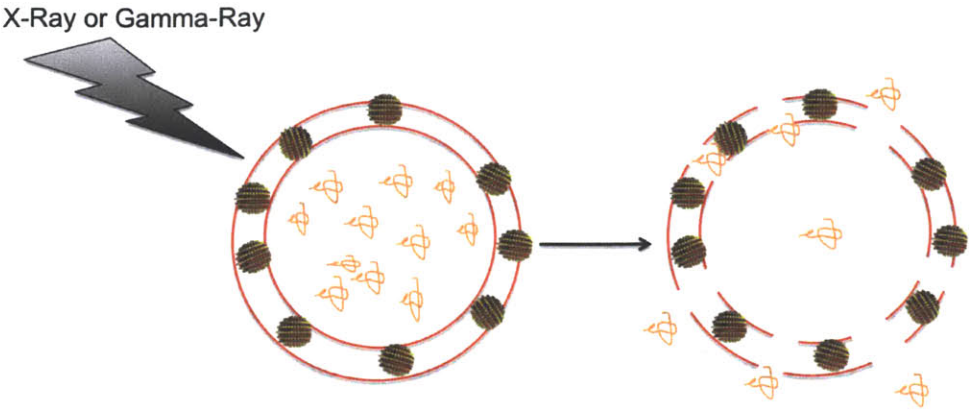

Figure 5-3: Illustration of gold nanoparticle-decorated lipid vesicles triggered drug release upon radiation treatment.

5.2 Experimental Methods

5.2.1 γ-ray Irradiator

Treated cells were washed twice with PBS and kept on ice at all times except when in the irradiator. Cells were treated with 4 gray (400 rads) of gamma radiation. The gamma cell irradiator (gammacell® 40 Exactor) used Cs^{137} source. Immediately after irradiation, cells were kept in a 37°C 5% CO_2 incubator for 3 hours to allow post-irradiation membrane damage to occur and then processed for flow cytometry fluorescence quantification analysis.

5.2.2 Flow Cytometry

Cells were seeded on a 24 well plate using 120,000 cells per well and allowed to attach overnight. 1uM of gold nanoparticles (soluble Au) or 1uM gold nanoparticles and 0.42 mM lipids (ICMV-Au) were incubated with the cells for 18 hours at 37 °C. Cell medium containing gold nanoparticles was removed and the wells were washed twice with icy cold PBS. Cells were trypsinized and transferred to a 96-U bottom plate for centrifugation at 1300 rpm for 5 minutes. Cells were resuspended in FACS buffer (PBS + 1% BSA) and kept on ice. Optionally, 5uL/mL of 1mg/mL DAPI was added to each well for dead cell-stain.

5.2.3 Clonogenic Assay

Clonogenic assay is a cell survival assay quantifying the ability of a single cell to grow into a colony. A colony consists of at least 50 cells. The assay tests every cell in the population for its ability to undergo unlimited proliferation. Clonogenic assay provided a way to determine cell reproductive death after treatment with ionizing radiation [17].

Cells were trypsinized and seeded immediately after radiation treatment, then grown in cell culture medium at 37°C for one week. Fixing, staining and clone-counting were performed after the week of growth. Cells counts in the resulting suspension were performed using a hemocytometer, and diluted in sterile tubes so as to pipet 100 up to 400 cells after treatment into the cell culture 6-wells. After one week of culture, cell medium was removed and cells were rinsed with PBS twice. 2 ml of a mixture of 6.0% glutaraldehyde and 0.5% crystal violet was added to each well and left in 4 ^{o}C for 30 minutes. The glutaraldehyde crystal violet mixture was carefully immersed in tap water until all excess dye was removed. The plates with colonies were air-dried at room temperature. Clones with more than 50 cells were counted using a stereomicroscope.

Different cell lines have different plating efficiencies. When untreated cells are plated as a single-cell suspension at low densities of 2–50 cells cm^2, they grow to colonies. Plating Efficiency (PE) is the ratio of the number of colonies to the number of cells seeded:

$$PE = \frac{\#\text{ colonies formed}}{\#\text{ cells seeded}} \times 100\%$$

The number of colonies that arise after treatment of cells, expressed in terms of PE, is called the surviving fraction (SF):

$$SF = \frac{\#\text{ colonies formed after treatment}}{\#\text{ cells seeded} \times PE} \times 100\%$$

5.3 Results and Discussion

5.3.1 Radiation Induced Membrane Damage in the Immediate Vicinity of Au Nanoparticles

Irradiation incident on aqueous solutions induces radiolysis of water, creating localized concentrations of highly reactive species (hydroxyl, peroxide, etc.) which cause damage to cellular structures including

protein and nucleic acids [34]. Cellular irradiation effects include induction of apoptosis, membrane rupture induced necrosis, and genomic damage. The killing efficiency of radiotherapy is dependent on cell type, radiation type, radiation energy, cumulative dose, dose rate, aqueous species concentrations, and the presence of radiosensitizers.

Radiosensitization of cellular membranes via gold nanoparticle decoration can be accomplished by incubation with aqueous gold nanoparticles or gold nanoparticle decorated ICMVs. Gold nanoparticles embedded in the outermost cell membranes may enhance local ionizing radiation damage, potentially increasing the probability of cell death. Quantification of radiosensitization efficacy was accomplished by comparison of fluorescence of live cells expressing GFP to dead cells stained with DAPI.

In the following figures (5-4 and 5-5), data is presented for irradiation of B16F10 and 4T1 cells treated with irradiation only, soluble gold nanoparticles, ICMV-gold, and gold-free ICMV control.

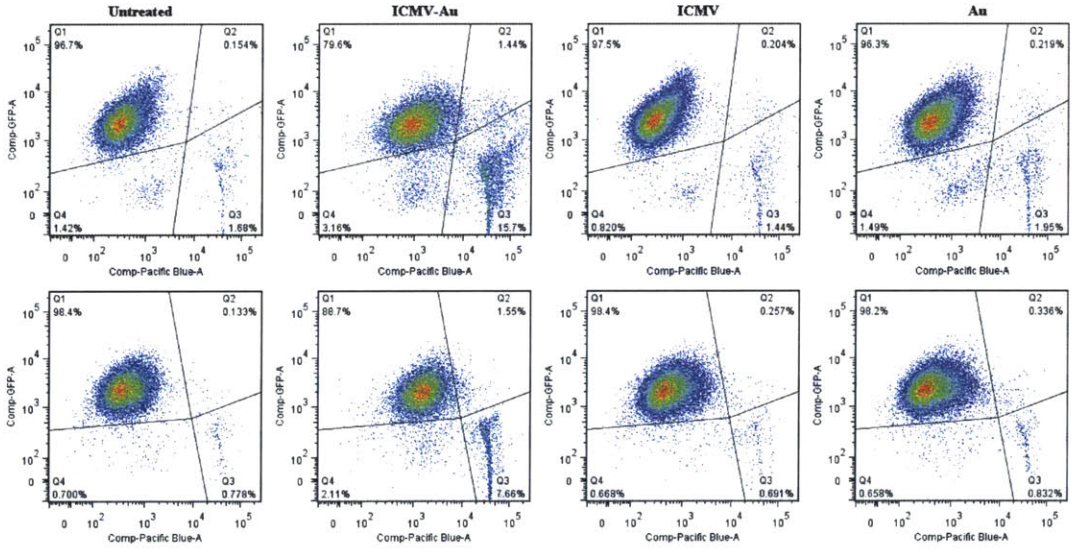

Figure 5-4: Membrane disruption quantification after of B16F10 cells. Irradiated cells (upper panel) and non-irradiated control cells (lower panel) were compared.

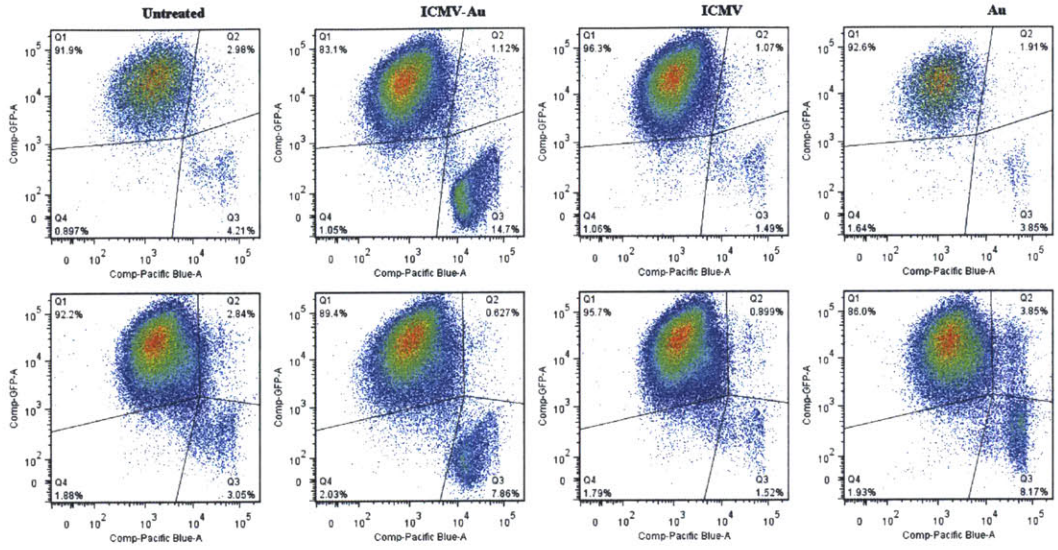

Figure 5-5: Membrane disruption quantification after of 4T1 Cells. Irradiated cells (upper panel) and non-irradiated control cells (lower panel) were compared.

ICMV-gold increase the killing efficiency by approximately one order of magnitude for B16F10 cells compared to soluble gold nanoparticles. ICMV-gold also increased cell death in non-irradiated B16F10, implying toxicity. The cause of ICMV-gold toxicity may be high concentration of lipids or the relatively large size of ICMV-gold.

4T1 cells followed the same trend however the killing efficiency enhancement was less pronounced—four-fold in comparison to the ten-fold increase in killing efficiency observed in ICMV-gold treated B16F10.

To examine the correlation between dead cells and gold nanoparticle uptake, an experiment was repeated expect that dye-labeled gold nanoparticles were used instead of non-dye-labeled gold nanoparticles. Membrane disrupted cells contained significantly more of gold nanoparticles then cells with intact membranes continuing to emit GFP. This phenomenon was observed in both B16F10 and 4T1 cell types (Figure 5-6 and 5-7).

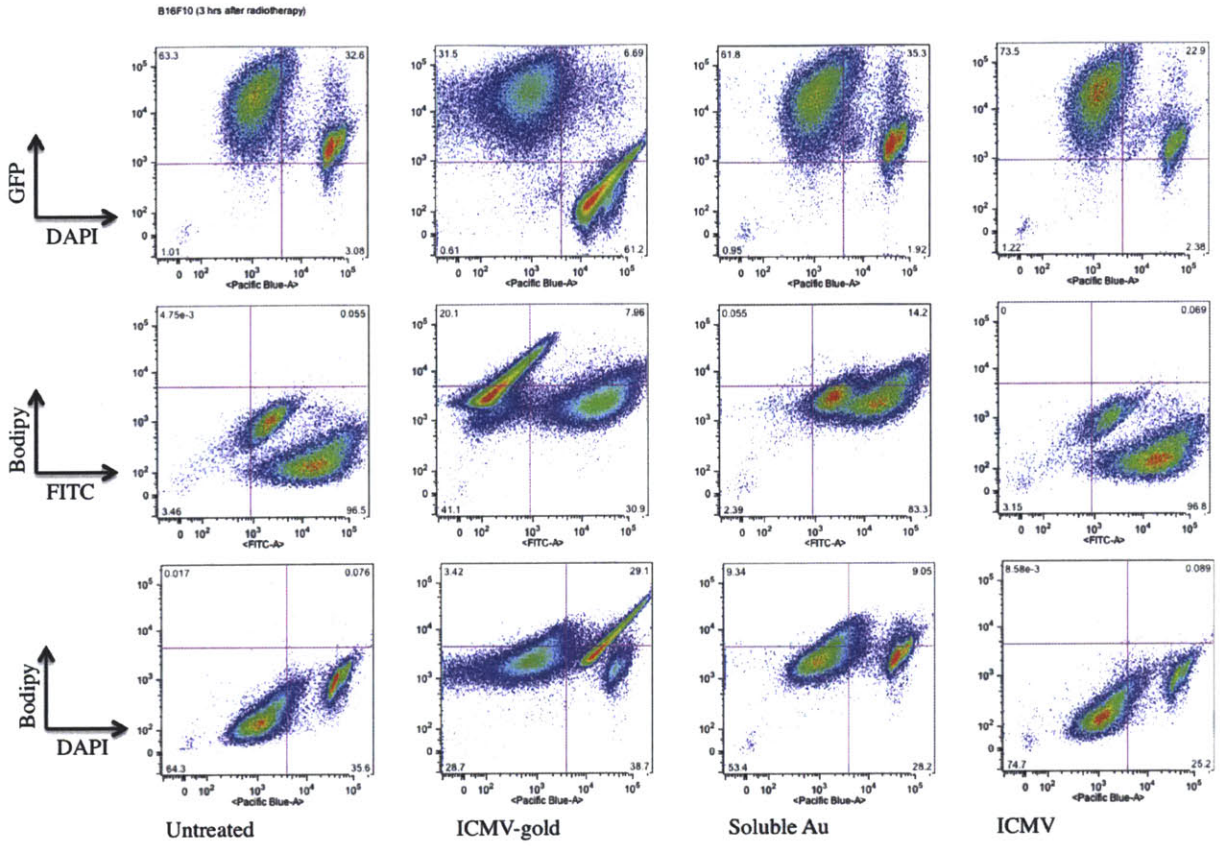

Figure 5-6: Dye labeled gold nanoparticles used in the study for the membrane disruption quantification after of B16F10 cells. Irradiated cells (upper panel) and non-irradiated control cells (lower panel) were compared.

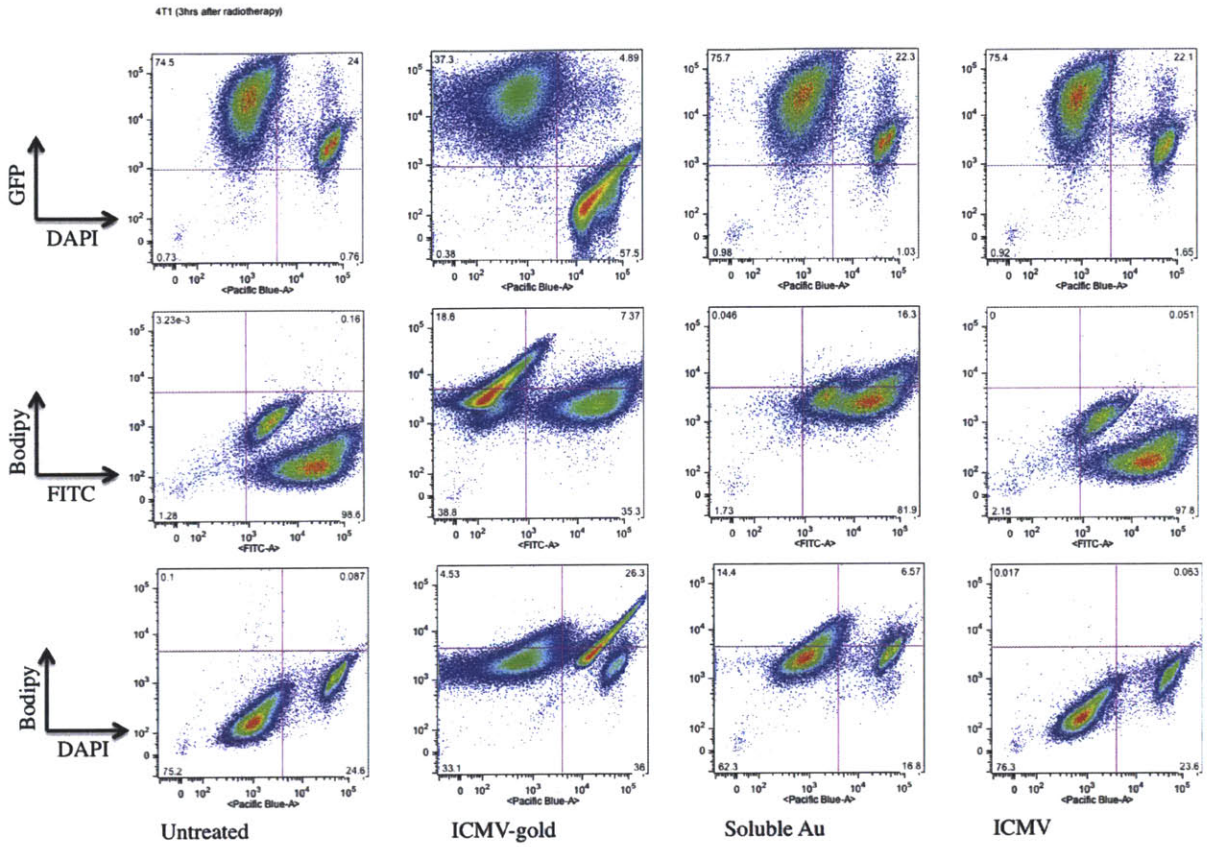

Figure 5-7: Dye labeled gold nanoparticles used in the study for the membrane disruption quantification after of 4T1 cells. Irradiated cells (upper panel) and non-irradiated control cells (lower panel) were compared.

5.3.2 Genomic Damage via Secondary Ionizing Radiation

The above mentioned radiolytic effects of irradiation are not confined to cellular membranes. Intra-cellular structures, compartments, and macromolecules may also be subjected to localized concentrations of reactive radicals resulting from interaction of incident irradiation with gold nanoparticles. Of particular interest is the probability and extent of genomic damage as a function of gold nanoparticle delivery mechanism (soluble vs. ICMV). Irradiation sufficient to cause genomic damage but not membrane rupture will negatively alter the proliferation profile of immortalized cell lines. To determine the efficacy of radiosensitization via soluble and ICMV-gold nanoparticles, irradiations were conducted to 4 Gy and a clonogenic assay was used to assess DNA damage. Untreated irradiations were also conducted.

The normalized survival fraction is the quantitative measure of a single cell's ability to grow into a colony post-treatment. Given the proper incubation environment, any reduction in this quantity for immortalized cell lines necessarily implies genomic damage has occurred as the result of irradiation.

The clonogenic assay (Figure 5-9) determined that genomic damage is cell type dependent. The post-irradiation loss of proliferation ability for untreated, soluble gold nanoparticles treated, and ICMV-gold treated B16F10 cells were 40%, 60%, and 72%, respectively (Figure 5-10). Gold nanoparticle killing efficiency was enhanced via ICMV delivery.

4T1 results were inconclusive because untreated irradiated cells had a lower normalized survival fraction than soluble gold nanoparticle treated cells (Figure 5-10). All irradiated cells had normalized survival fractions within one standard deviation, regardless of treatment. One possible explanation for this would be extreme susceptibility of 4T1 cells to radiolysis.

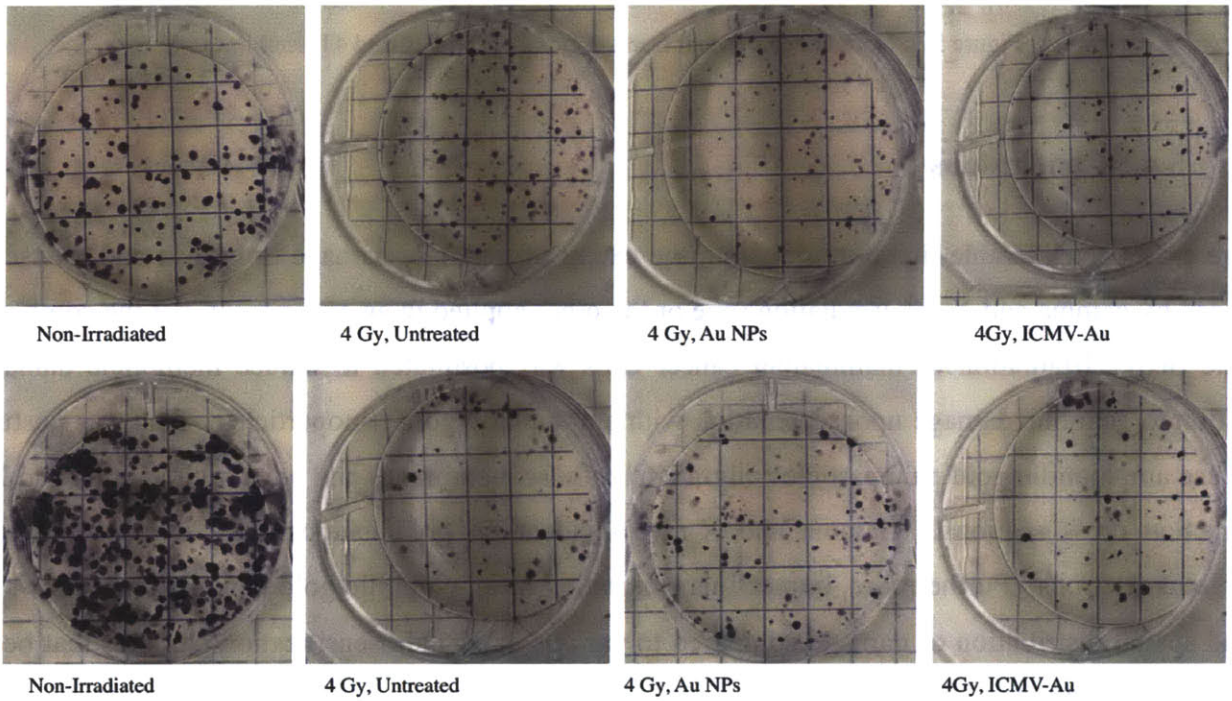

Figure 5-8: Clonogenic assay of B16F10 (upper panel) and 4T1 (lower panel) cells after radiation therapy.

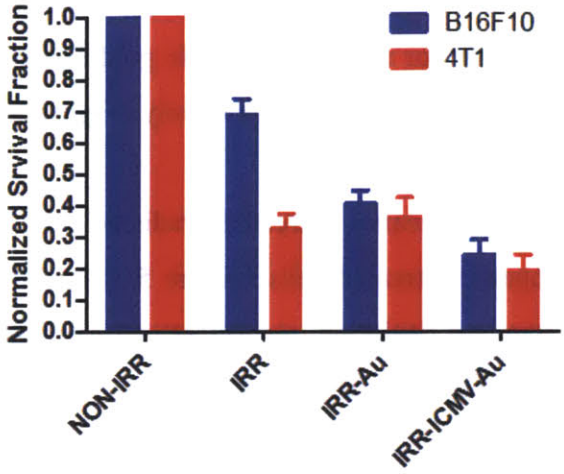

Figure 5-9: Normalized survival fraction curve of B16F10 and 4T1 cell lines.

5.4 Conclusions

There exists considerable literature detailing the extent of genomic damage to human and mouse cells induced by gamma and X-ray irradiation (one or the other applied in an experiment, not the combination of the two). Irradiation of mammalian cancer cells was postulated to induce membrane damage in addition to genomic damage upon decoration with amphiphilic gold nanoparticles. This was postulated because amphiphilic gold nanoparticles migrate to cellular membranes and have high gamma and X-ray interaction cross sections. Gamma and X-rays incident on gold nanoparticles induce emission of energetic electrons. Furthermore, intracellular migration of amphiphilic gold nanoparticles allows for a broad spatial distribution of damage compared to various other radiosensitization particles that become confined in endosomes.

Membrane damage was observed in post-irradiation ICMV-Au treated cells. Membrane damage was not observed in post-irradiation soluble Au treated cells. Genomic damage was also observed in post-irradiation ICMV-Au treated cells. Less genomic damage was observed in post-irradiation soluble Au treated cells. The efficacy of amphiphilic gold nanoparticle radiosensitization was observed experimentally to be a function of cellular gold nanoparticle concentration. Cellular gold nanoparticle concentration was increased via utilization of ICMVs as an amphiphilic gold nanoparticle vector. ICMV-Au was observed to exhibit toxicity, killing non-irradiated cells. Further experimentation is required to determine toxicity thresholds.

Irradiation damage is postulated to be source dependent. According to established literature the energy of incident radiation strongly affects the energy transferred when interacting with Au [28]. Future work currently in progress in this area may show that irradiation via 80 kV X-ray is more efficacious than gamma ray irradiation.

6 Conclusions

6.1 Thesis Summary

Striped gold nanoparticles are a recent evolution of intracellular delivery vectors. These nanoparticles have a variety of properties that enable their application to a range of biomedical clinical treatments. Their surfaces can be functionalized by the conjugation of thiol-terminated cargos. They have a high atomic number which results in a high interaction cross section with electromagnetic radiation. They are capable of simultaneously binding hydrophobic and hydrophilic compounds. They are also soluble in lipid bilayers, in many cases migrating between adjacent bilayers or causing bilayer fusion. This bilayer solubility also may allow striped gold nanoparticles to serve as a vector for delivery of hydrophobic drugs to bacteria. We showed here that striped gold nanoparticles bind to the external membranes of *E. Coli* and *Salmonella*.

Bilayer vesicles present in natural cells serve a variety of functions, and are therefore readily adapted to clinical applications. Lipid bilayers can be synthesized from a variety of different lipids and combinations of lipids. Multilamellar vesicles can be synthesized, and cross-linked to form ICMVs. Considerable variation exists in lipid chemistry affecting vesicle shape, size, and solvent properties for solutes including proteins and gold nanoparticles. Decoration of lipid bilayers with gold nanoparticles allows for the development of manifold applications including pharmaceutical delivery, radiosensitization, and both. Synthesis and size control of an efficacious gold nanoparticle decorated vesicle was realized with the ICMV-Au. This development facilitated a means to the delivery of highly concentrated gold nanoparticles simultaneously with desired chemodrugs or vaccines. One potential application would be *in vivo* tissue sectioning of ICMV targeted sites using electron microscopy.

Synthetic lipid membrane interaction with striped gold nanoparticles demonstrated PEG was not an effective surface protector for the inhibition of striped nanoparticles' non-specific interaction with membranes. Striped gold nanoparticles penetrated all tested synthetic lipid membranes, including DOPC, DOPG, DOPE-PEG, and DSPE-PEG. Gold nanoparticles on liposomes, MLVs, or ICMVs migrated to adjacent model cell membranes without membrane rupture. The result suggested a promising property of membrane penetration for intracellular delivery of gold nanoparticles.

ICMV-Au was shown to enhance killing efficiency of *in vitro* radiation therapy, by both damage of cell membrane and DNA. Radiosensitivity is cell line dependent. Significant gold nanoparticles aided membrane disruption induced cell death was observed in both B16F10 and 4T1 cells, while genomic damage enhancement by gold nanoparticles was only observed in B16F10 cell lines. The ultimate goal of this research is simultaneous chemo/radio therapeutic cancer treatment. Gold nanoparticle-decorated ICMVs developed in this study comprised a new vector for the efficacious co-delivery of membrane interactive nanoparticles and pharmaceuticals.

6.2 Future Perspectives

Membrane interactive amphiphilic gold nanoparticles interact with lipid membranes and have been shown to penetrate a variety of lipid membranes. Despite the fact that they possess advantageous cytosolic distribution due to their ease of membrane migration, efficacious delivery *in vivo* requires gold nanoparticles to be trapped in the original bilayers before they reach targeted sites. In other work in our laboratory, it was found that amphiphilic gold nanoparticles were not able to penetrate the bilayers of high-T_m lipid vesicles. Gold nanoparticles incorporated in high-T_m lipid vesicles may be trapped inside the vesicles. Stealth high T_m lipid vesicles may trap gold nanoparticles and block non-specific interaction with vicinity membranes systemically until they reach targeted sites. Intracellular lipid vesicles degradation may limit nanoparticle distribution to the endocytotic cell. Highly localized nanoparticles distributions of this nature may prove highly efficacious for clinical applications. Therefore, we envision that synthesis of gold nanoparticle-incorporated high T_m ICMVs or liposomes for efficient *in vivo* gold nanoparticles targeted delivery is warranted.

To further increase the efficacy of radiosensitization, parameters such as irradiation sources, dose rate, concentration of ICMV-Au treated should be optimized. *In vivo* biodistribution of ICMV-Au should be investigated for passive tumor targeting treatment. Implementation of ICMV-Au vectors *in vivo* may one day significantly advance the state of the art of modern cancer treatment.

References

[1] Akin, D. *et al.* Bacteria-mediated delivery of nanoparticles and cargo into cells. *Nature Nanotechnology* **2**, 441-449, doi:10.1038/nnano.2007.149 (2007).

[2] Alkilany, A. M. & Murphy, C. J. Toxicity and cellular uptake of gold nanoparticles: what we have learned so far? *Journal of Nanoparticle Research* **12**, 2313-2333, doi:10.1007/s11051-010-9911-8 (2010).

[3] Almeida, J. P. M., Chen, A. L., Foster, A. & Drezek, R. In vivo biodistribution of nanoparticles. *Nanomedicine* **6**, 815-835, doi:10.2217/nnm.11.79 (2011).

[4] Arifin, D. R. & Palmer, A. F. Physical properties and stability mechanisms of poly(ethylene glycol) conjugated liposome encapsulated hemoglobin dispersions. *Artificial Cells Blood Substitutes and Biotechnology* **33**, 137-162, doi:10.1081/bio-200055880 (2005).

[5] Acharya, S. & Sahoo, S. K. PLGA nanoparticles containing various anticancer agents and tumor delivery by EPR effect. *Advanced Drug Delivery Reviews* **63**, 170-183, doi:10.1016/j.addr.2010.10.008 (2011).

[6] Ackerson, C. J., Jadzinsky, P. D. & Kornberg, R. D. Thiolate ligands for synthesis of water-soluble gold clusters. *Journal of the American Chemical Society* **127**, 6550-6551, doi:10.1021/ja046114i (2005).

[7] Balasubramanian, S. K. *et al.* Biodistribution of gold nanoparticles and gene expression changes in the liver and spleen after intravenous administration in rats. *Biomaterials* **31**, 2034-2042, doi:10.1016/j.biomaterials.2009.11.079 (2010).

[8] Allen, T. M., Hansen, C., Martin, F., Redemann, C. & Yauyoung, A. LIPOSOMES CONTAINING SYNTHETIC LIPID DERIVATIVES OF POLY(ETHYLENE GLYCOL) SHOW PROLONGED CIRCULATION HALF-LIVES INVIVO. *Biochimica Et Biophysica Acta* **1066**, 29-36, doi:10.1016/0005-2736(91)90246-5 (1991).

[9] Chen, H. *et al.* In Vivo Study of Spherical Gold Nanoparticles: Inflammatory Effects and Distribution in Mice. *Plos One* **8**, doi:10.1371/journal.pone.0058208 (2013).

[10] Chithrani, B. D., Ghazani, A. A. & Chan, W. C. W. Determining the size and shape dependence of gold nanoparticle uptake into mammalian cells. *Nano Letters* **6**, 662-668, doi:10.1021/nl052396o (2006).

[11] Chithrani, D. B. *et al.* Gold Nanoparticles as Radiation Sensitizers in Cancer Therapy. *Radiation Research* **173**, 719-728, doi:10.1667/rr1984.1 (2010).

[12] Chithrani, D. B., Dunne, M., Stewart, J., Allen, C. & Jaffray, D. A. Cellular uptake and transport of gold nanoparticles incorporated in a liposomal carrier'. *Nanomedicine-Nanotechnology Biology and Medicine* **6**, 161-169, doi:10.1016/j.nano.2009.04.009 (2010).

[13] Chou, L. Y. T., Ming, K. & Chan, W. C. W. Strategies for the intracellular delivery of nanoparticles. *Chemical Society Reviews* **40**, 233-245, doi:10.1039/c0cs00003e (2011).

[14] Daniel, M. C. & Astruc, D. Gold nanoparticles: Assembly, supramolecular chemistry, quantum-size-related properties, and applications toward biology, catalysis, and nanotechnology. *Chemical Reviews* **104**, 293-346, doi:10.1021/cr030698+ (2004).

[15] De Jong, W. H. *et al.* Particle size-dependent organ distribution of gold nanoparticles after intravenous administration. *Biomaterials* **29**, 1912-1919, doi:10.1016/j.biomaterials.2007.12.037 (2008).

[16] Dietrich, G. Bacteria give nanoparticles a ride. *Nature Nanotechnology* **2**, 394-395, doi:10.1038/nnano.2007.161 (2007).

[17] Franken, N. A. P., Rodermond, H. M., Stap, J., Haveman, J. & van Bree, C. Clonogenic assay of cells in vitro. *Nature Protocols* **1**, 2315-2319, doi:10.1038/nprot.2006.339 (2006).

[18] Giljohann, D. A. *et al.* Gold Nanoparticles for Biology and Medicine. *Angewandte Chemie-International Edition* **49**, 3280-3294, doi:10.1002/anie.200904359 (2010).

[19] Hainfeld, J. F., Dilmanian, F. A., Slatkin, D. N. & Smilowitz, H. M. Radiotherapy enhancement with gold nanoparticles. *Journal of Pharmacy and Pharmacology* **60**, 977-985, doi:10.1211/jpp.60.8.0005 (2008).

[20] Hainfeld, J. F. *et al.* Gold nanoparticles enhance the radiation therapy of a murine squamous cell carcinoma. *Physics in Medicine and Biology* **55**, 3045-3059, doi:10.1088/0031-9155/55/11/004 (2010).

[21] Hainfeld, J. F., Slatkin, D. N. & Smilowitz, H. M. The use of gold nanoparticles to enhance radiotherapy in mice. *Physics in Medicine and Biology* **49**, N309-N315, doi:10.1088/0031-9155/49/18/n03 (2004).

[22] Halliwell, B. & Aruoma, O. I. DNA Damage by Oxygen-derived Species -Its Mechanism and Measurement in Mammalian Systems. *Febs Letters* **281**, 9-19, doi:10.1016/0014-5793(91)80347-6 (1991).

[23] Han, G., Ghosh, P. & Rotello, V. M. Functionalized gold nanoparticles for drug delivery. *Nanomedicine* **2**, 113-123, doi:10.2217/17435889.2.1.113 (2007).

[24] Hirsch, L. R. *et al.* Nanoshell-mediated near-infrared thermal therapy of tumors under magnetic resonance guidance. *Proceedings of the National Academy of Sciences of the United States of America* **100**, 13549-13554, doi:10.1073/pnas.2232479100 (2003).

[25] Huang, X. H., Jain, P. K., El-Sayed, I. H. & El-Sayed, M. A. Gold nanoparticles: interesting optical properties and recent applications in cancer diagnostic and therapy. *Nanomedicine* **2**, 681-693, doi:10.2217/17435889.2.5.681 (2007).

[26] Jewell, C. M. *et al.* Oligonucleotide Delivery by Cell-Penetrating "Striped" Nanoparticles. *Angewandte Chemie-International Edition* **50**, 12312-12315, doi:10.1002/anie.201104514 (2011).

[27] Jain, S. *et al.* Cell-specific Radiosensitization by Gold Nanoparticles Nanoparticles by Gold Nanoparticles at Megavoltage Radiation Energies. *International Journal of Radiation Oncology Biology Physics* **79**, 531-539, doi:10.1016/j.ijrobp.2010.08.044 (2011).

[28] Jain, S., Hirst, D. G. & O'Sullivan, J. M. Gold nanoparticles as novel agents for cancer therapy. *British Journal of Radiology* **85**, 101-113, doi:10.1259/bjr/59448833 (2012).

[29] Jackson, A. M., Myerson, J. W. & Stellacci, F. Spontaneous assembly of subnanometre-ordered domains in the ligand shell of monolayer-protected nanoparticles. *Nature Materials* **3**, 330-336, doi:10.1038/nmat1116 (2004).

[30] Khlebtsov, N. & Dykman, L. Biodistribution and toxicity of engineered gold nanoparticles: a review of in vitro and in vivo studies. *Chemical Society Reviews* **40**, 1647-1671, doi:10.1039/c0cs00018c (2011).

[31] Kim, C. K. *et al.* Entrapment of Hydrophobic Drugs in Nanoparticle Monolayers with Efficient Release into Cancer Cells. *Journal of the American Chemical Society* **131**, 1360-+, doi:10.1021/ja808137c (2009).

[32] Lipka, J. *et al.* Biodistribution of PEG-modified gold nanoparticles following intratracheal instillation and intravenous injection. *Biomaterials* **31**, 6574-6581, doi:10.1016/j.biomaterials.2010.05.009 (2010).

[33] Maeda, H. The enhanced permeability and retention (EPR) effect in tumor vasculature: The key role of tumor-selective macromolecular drug targeting. *Advances in Enzyme Regulation, Vol 41* **41**, 189-207, doi:10.1016/s0065-2571(00)00013-3 (2001).

[34] Mishra, K. P. Cell membrane oxidative damage induced by gamma-radiation and apoptotic sensitivity. *Journal of Environmental Pathology Toxicology and Oncology* **23**, 61-66, doi:10.1615/JEnvPathToxOncol.v23.i1.60 (2004).

[35] Moon, J. J. *et al.* Interbilayer-crosslinked multilamellar vesicles as synthetic vaccines for potent humoral and cellular immune responses. *Nature Materials* **10**, 243-251, doi:10.1038/nmat2960 (2011).

[36] Nativo, P., Prior, I. A. & Brust, M. Uptake and intracellular fate of surface-modified gold nanoparticles. *Acs Nano* **2**, 1639-1644, doi:10.1021/nn800330a (2008).

[37] Pan, Y. *et al.* Size-dependent cytotoxicity of gold nanoparticles. *Small* **3**, 1941-1949, doi:10.1002/smll.200700378 (2007).

[38] Paciotti, G. F., Kingston, D. G. I. & Tamarkin, L. Colloidal gold nanoparticles: A novel nanoparticle platform for developing multifunctional tumor-targeted drug delivery vectors. *Drug Development Research* **67**, 47-54, doi:10.1002/ddr.20066 (2006).

[39] Prakash, S., Malhotra, M., Shao, W., Tomaro-Duchesneau, C. & Abbasi, S. Polymeric nanohybrids and functionalized carbon nanotubes as drug delivery carriers for cancer therapy. *Advanced Drug Delivery Reviews* **63**, 1340-1351, doi:10.1016/j.addr.2011.06.013 (2011).

[40] Radovic-Moreno, A. F. *et al.* Surface Charge-Switching Polymeric Nanoparticles for Bacterial Cell Wall-Targeted Delivery of Antibiotics. *Acs Nano* **6**, 4279-4287, doi:10.1021/nn3008383 (2012).

[41] Sonavane, G., Tomoda, K. & Makino, K. Biodistribution of colloidal gold nanoparticles after intravenous administration: Effect of particle size. *Colloids and Surfaces B-Biointerfaces* **66**, 274-280, doi:10.1016/j.colsurfb.2008.07.004 (2008).

[42] Singh, C. *et al.* Entropy-mediated patterning of surfactant-coated nanoparticles and surfaces. *Physical Review Letters* **99**, 4, doi:10.1103/PhysRevLett.99.226106 (2007).

[43] Stegh, A. H. Toward personalized cancer nanomedicine - past, present, and future. *Integrative Biology* **5**, 48-65, doi:10.1039/c2ib20104f (2013).

[44] Torchilin, V. P. Recent advances with liposomes as pharmaceutical carriers. *Nature Reviews Drug Discovery* **4**, 145-160, doi:10.1038/nrd1632 (2005).

[45] Verma, A. *et al.* Surface-structure-regulated cell-membrane penetration by monolayer-protected nanoparticles. *Nature Materials* **7**, 588-595, doi:10.1038/nmat2202 (2008).

[46] Xiu, Z. M., Zhang, Q. B., Puppala, H. L., Colvin, V. L. & Alvarez, P. J. J. Negligible Particle-Specific Antibacterial Activity of Silver Nanoparticles. *Nano Letters* **12**, 4271-4275, doi:10.1021/nl301934w (2012).

[47] Yoon, H., Ansong, C., Adkins, J. N. & Heffron, F. Discovery of Salmonella Virulence Factors Translocated via Outer Membrane Vesicles to Murine Macrophages. *Infection and Immunity* **79**, 2182-2192, doi:10.1128/iai.01277-10 (2011).